



i⁸th iceast 2022

Chiang Mai, Thailand

8-10 JUNE 2022

<http://iceast2022.iceast.info/>

Conference Proceeding

Table of Contents

Message from Honorary Chairs	III
Message from General Chairs	VI
Message from Technical Program Chairs	VII
Organizing Committee	VIII
Proceeding	
Application of Fast Fourier Transform to the Synthesis of Track Irregularities	1
<p>Panya Kansuwan <i>(King Mongkut's Institute of Technology Ladkrabang, Bangkok, Thailand)</i> Sedthawat Sucharitpwatskul and Anchalee Manonukul <i>(National Science and Technology Development Agency, Pathumthani, Thailand)</i></p>	
Eco-Efficiency of Smart Reclaimed water management system: A case study of wastewater treatment from natural rubber processing (Condom Production)	11
<p>Phisuttinee Poolchantakorn, Jakkapong Chupayak, Brian Youichi Kempimook, Preecha Supina, Oumaporn Tesiri <i>(Thai Nippon Rubber Industry Public Company Limited Si Racha District, Chon Buri, Thailand)</i> Surachai Wongcharee <i>(Mahasarakham University, Mahasarakham, Thailand)</i> Torpong Kreetachart <i>(University of Phayao, Phayao, Thailand)</i> Supatta Chueycham, Taddao Pahasup-anan, Kowit Suwannahong <i>(University Chon Buri, Thailand)</i></p>	
Drying of Unripe Banana (<i>Musa sapientum</i> Linn.) Using Microwave Combined with Hot Air	22
<p>Nattapol Poomsa-ad and Lamul Wiset <i>(Mahasarakham University Maha Sarakham, Thailand)</i></p>	
Development of Fiber Stripping Machine for Eri Cocoon	31
<p>Kasorn Wongkasem, Surachai Wongcharee, Pitak Promthaisong, Kaned Toong-ood <i>(Mahasarakham University Mahasarakham, Thailand)</i> Nantawatana Weerayuth <i>(Ubonratchathanee University Ubonratchathanee, Thailand)</i></p>	
A Study on The Effects of Natural-Rubber and Concrete Panel Railroad Crossing Using Finite Element Method	39
<p>Sirawit Pettrueang and Monsak Pimsarn <i>(King Mongkut's Institute of Technology Ladkrabang, Bangkok, Thailand)</i></p>	
Thermal Comfort Characteristics Using An Automatic Fan Speed Control And 360° Object Tracking Based On Microcontroller	50
<p>Jindaporn Jamradloedluk and Songchai Wiriyaumpaiwong <i>(Mahasarakham University Maha Sarakham, Thailand)</i></p>	

Automatic Shrimp Size Measurement for Pacific White Shrimp Farming Industry 59
Using Artificial Intelligence
Charoen Vongchumyen, Nachaphat Ainthong, Poramee Chansuksett, Charita Suranantajak
(*King Mongkut's Institute of Technology Ladkrabang, Bangkok, Thailand*)

Author index 68

Message from Honorary Chairs



It is my great pleasure to welcome you to the 8th International Conference on Engineering, Applied Sciences and Technology (ICEAST 2022). This year conference format is different from those in the preceding years in that it is organized online due to the covid-19 pandemic. Despite this difficulty, the aim of the conference remains the same that it strives to provide a platform for participants to gather the latest knowledge in engineering and applied science, and an opportunity for enhancing collaboration.

I would like to extend my special thanks to the conference staff, participants, session chairs, and keynote speaker for helping to create this exciting conference program. I hope this event will be the starting point of collaborative partnership creation and innovation community building.

Finally, I wish you all every success in ICEAST 2022.

Anuwat Jangwanitlert

President (Acting)

King Mongkut's Institute of Technology Ladkrabang (KMITL), Thailand

Message from Honorary Chairs



Welcome to the 8th International Conference on Engineering, Applied Sciences and Technology (ICEAST 2022). The conference has been held annually and is the one of the world premier technical events covering the entire aspects of engineering, technology, applied sciences and current interdisciplinary across all topics focusing on the diverse applications. The KMITL School of Engineering is dedicated to research and training in engineering and technological disciplines looking to provide opportunities for enchanting networking, collaboration and exploring current interdisciplinary topics. We are highly delighted to be a part of this technological networking platform, though the ICEAST 2022 has been shifted to a fully virtual conference. We truly believe that the conference will be successful and meet the targeted goals.

On behalf on the honorary chair, I welcome you all to the 8th International Conference of Engineering, Applied Sciences and Technology (ICEAST 2022) and hope that you have a great time knowledge transferring and networking between participants and are rewarded by the technical challenges of the ICEAST 2022.

A handwritten signature in blue ink, appearing to read 'Somyot K.' with a stylized flourish at the end.

Somyot Kiatwanidvilai

Dean of School of Engineering
King Mongkut's Institute of Technology Ladkrabang (KMITL), Thailand

Message from Honorary Chairs



The Institute of Electrical and Electronics Engineers (IEEE) is the world's largest technical professional society. Founded in 1884 by a handful of practitioners of the new electrical engineering discipline, today's institute is comprised of more than 320,000 members who conduct and participate in its activities in 147 countries. The men and women of the IEEE are the technical and scientific professionals making the revolutionary engineering advances which are reshaping our world today.

It is my great honor to welcome all participants to the 6th International Conference on Engineering, Applied Sciences and Technology (ICEAST 2022). I would like to express my sincere thank to the organizing committees for hosting the conference. I am also deeply indebted to general chair of ICEAST 2022, Dr. Sathaporn Promwong, for making this virtual conference possible.

Finally, I wish all attendants have a productive time in the conference and continue to contribute to the success of ICEAST in the years to come.

Pongsakorn Yuthagovit
President of IEEE Thailand Section

Message from General Chairs



It is my honor to welcome you to the 8th International Conference on Engineering, Applied Sciences and Technology (ICEAST 2022). To comply with the social distancing rule brought on by covid-19 pandemic, this year conference program is held online at the King Mongkut's Institute of Technology Ladkrabang (KMITL), Bangkok, Thailand. It is co-organized by the Institute of Electrical and Electronics Engineers (IEEE).

I would like to express my gratitude toward the keynote speaker and participants. I also would like to extend my congratulations to the authors and presenters. This conference would not have been successful without the support from our sponsors and we greatly appreciate their contributions. I hope that this conference will provide not only outstanding technical knowledge but also enjoyable experience for the participants. In conclusion, I am delighted to give a warm welcome to all you.

I am very grateful to all my colleagues who help make this virtual conference possible. I appreciate all the participants for their contributions to the success of ICEAST 2022. I hope their efforts will be rewarded and the conference will meet everyone's expectations.

Sathaporn Promwong

General Chair
IEEE BTS Chapter Chair

Message from Technical Program Chairs



On behalf of the Technical Program Committee (TPC), it is my great pleasure to welcome you all to participate in the 8th International Conference on Engineering, Applied Sciences and Technology (ICEAST 2022).

ICEAST 2022 is intended to provide an international forum where researchers and practitioners interested in the advancement of engineering, applied sciences and technology can exchange the latest research results and ideas through presentation and discussion. This year we have received 99 papers from various countries. After the rigorous review process, only 45 papers have been accepted with the acceptance rate of 45.45 %. The technical program of ICEAST 2022 consists of 2 keynote sessions and 9 oral presentation sessions.

I would like to express my gratitude toward the keynote speaker and participants. I also would like to extend my congratulations to the authors and presenters. This conference would not have been successful without the support from our sponsors and we greatly appreciate their contributions. I hope that this conference will provide not only outstanding technical knowledge but also enjoyable experience for the participants. In conclusion, I am delighted to give a warm welcome to all you.

Norasage Pattanadech
Aditep Chaisang

Technical Program Chairs

Organizing Committee

Honorary Chair

- Anuwat Jangwanitlert (KMITL, Thailand)
- Somyot Kaitwanidvilai (KMITL, Thailand)
- Khamphoui Southisombat (NUOL, Lao PDR)
- Pitak Thumwarin (KMITL, Thailand)
- Anantawat Kunakorn (KMITL, Thailand)
- Pongsakorn Yuthagovit (IEEE, Thailand)

General Chairs

- Sathaporn Promwong (KMITL & IEEE, Thailand)

Organizing-Chairs

- Chanin Bunlaksananusorn (KMITL, Thailand)

International Advisory Committee (IAC)

- Yoshikazu Miyataka (Hokkaido University, Japan)
- Takao Onoye (Osaka University, Japan)
- Kazuhiko Hamamoto (Tokai University, Japan)
- Rajeev Prasad (River Publishers, Denmark)
- Kyung Sup Kwak (Inha University, South Korea)
- Dusit Niyato (NTU, Singapore)
- Tadashi Ariga (Tokai University, Japan)
- Tomotaka Homae (NIT Toyama College, Japan)
- Nobutaka Ito (CMU, Thailand)
- Satoru Seto (NIT Ishikawa College, Japan)
- Kuniaki Yajima (NIT Sendai, Japan)
- Phonekeo Chanthamaly (NUOL, Lao PDR)
- Sengpasong Phrakonekham (NUOL, Lao PDR)
- Eryk Dutkiewicz (UTS, Australia)
- Myo Myint Maw (MTU, Myanmar)

ICEAST Steering Committee

- Wipoo Sriseubsai (KMITL, Thailand)
- Uma Seeboonruang (KMITL, Thailand)

- Chaowalit Hamontree (KMITL, Thailand)
- Worapong Tangsrirat (KMITL, Thailand)
- Chuwong Phongcharoenpanich (KMITL, Thailand)
- Sathaporn Promwong (KMITL & IEEE, Thailand)
- Wiboon Promphanich (KMITL, Thailand)
- Chanin Bunlaksananusorn (KMITL, Thailand)
- Norasage Pattanadech (KMITL, Thailand)
- Theerayod Wiangtong (KMITL, Thailand)
- Chayapol Khamyod (MFU, Thailand)
- Khamphoui Southisombat (NUOL, Lao PDR)
- Somsanouk Pathoumvanh (NUOL, Lao PDR)
- Khanthanou Luangxaysana (NUOL, Lao PDR)
- Myint Thein (YTU, Myanmar)
- Sint Soe (MTU, Myanmar)

Technical Program Chairs

- Norasage Pattanadech (KMITL, Thailand)
- Aditep Chaisang (RBRU, Thailand)

Technical Committee

- Phacharaphon Tunthawiroon (KMITL, Thailand)
- Monsak Pimsarn (KMITL, Thailand)
- Pornsawan Assawasaengrat (KMITL, Thailand)
- Pichaya Supanakoon (KMITL, Thailand)
- Nachanant Chitanont (KMITL, Thailand)
- Yoothana Suansook (DTI, Thailand)

Special Session Chairs

- Sawai Pongswatd (KMITL, Thailand)
- Suchada Sitjongsataporn (MUT, Thailand)
- Rachen Kanahna (PBRU, Thailand)
- Krittika Kantawong (UP, Thailand)

Publication Chair

- Kriangkrai Sooksood (KMITL, Thailand)
- Unnat Pinsopol (KMITL, Thailand)
- Chayapol Khamyod (MFU, Thailand)

-
- Thanadol Tiengthong (KMITL, Thailand)

Information System Chair/ Performance Publicity/ Public Relation Chairs

- Sarun Duangsuwan (KMITL, Thailand)
- Nattapan Suwansukho (KMITL, Thailand)
- Wipassorn Vinicchayakul (CATC, Thailand)

Financial Chair

- Wiboon Promphanich (KMITL, Thailand)
- Vidhya Rugpong (IEEE, Thailand)

Registration Chair

- Siripan Trakuldit (NSTRU, Thailand)
- Sanit Teawchim (KOSEN-KMITL, Thailand)
- Kittisak Thungsook (RMUTR, Thailand)

Sponsor & Exhibition Chair

- Suthee Suwannaprapha (MCOT, Thailand)
- Sakda Maneerot (TESLA POWER, Thailand)
- Thanadon Mankong (N&N, Thailand)

Local Arrangements Chairs

- Jirapat Sangthong (MUT, Thailand)
- Bundit Ruckveratham (MCOT, Thailand)
- Virot Wuti (KMITL, Thailand)
- Ammata Lhuangphon (KMITL, Thailand)

General Secretary

- Theerayod Wiangtong (KMITL, Thailand)

Application of Fast Fourier Transform to the Synthesis of Track Irregularities

Panya Kansuwan¹, Sedthawat Sucharitpwatskul² and Anchalee Manonukul²

¹*Mechanical Engineering Department, School of Engineering, King Mongkut's Institute of Technology Ladkrabang, Bangkok, Thailand*

²*National Metal and Materials Technology Center, National Science and Technology Development Agency, Pathumthani, Thailand*

E-mail address: panya.ka@kmitl.ac.th, sedthaws@mtec.or.th, anchalm@mtec.or.th

Abstract

The theoretical analysis of railway vehicles' dynamic behavior requires track models that include track irregularities. The power spectrum density (PSD) function is a well-accepted mathematical expression suitable for the irregular random nature. Since there are various PSD parameters according to the impact on the vehicles, track engineering quantifies track quality into six classes in the USA but two categories in Germany. EN13848 considers track irregularity at different wavelengths, while UIC518 classified the track quality as QN1, QN2, and QN3 by a standard deviation depending on the speeds of the rail vehicles. Minimum separated lengths of errors are also recommended. This paper presents a unified algorithm to synthesize the track irregularity conforming to each standard when PSD is provided with a standard deviation of the data, sample length, and track length. The algorithm implements the parameters in Discrete Fourier Transformation (DFT) representation, giving the availability to use Fast Fourier Transformation (FFT) that can speed up the computational time.

Keywords. track irregularity, power spectral density, rail vehicle dynamics, Discrete Fourier Transform, Fast Fourier Transform

1. INTRODUCTION

One system input that influences the rail vehicle dynamics is the track on which the vehicle runs. The track geometry is not plenary but contains intentionally and unintentionally variations described in four irregularities, i.e., cross-level, alignment, vertical, and gage track profile [1, 2]. Different classes of track quality exist depending on the influence of the parameters on track/vehicle interaction aspects such as vehicle performance, passenger

2

comfort, and safety issue analysis compared to a safety threshold. The Federal Railroad Administration (FRA) divides the track into six classes [3], whereas the German high-speed train engineers classify two classes of the track [2]. Depending on the speed of the vehicles, track quality in the European network is represented under three quality levels defined as QN1, QN2, and QN3 [4]. Due to the importance of the geometry variation, researchers and designers have studied two interrelated aspects of the subject, i.e., the measurement of track irregularities and the dynamic response behaviors of rail vehicles to the irregularity.

The first aspect states the design of the device structure to measure, record, and interpret the irregularity information. The track measurement devices range from human pushed trolleys to fully automated measuring Track Recording Vehicles (TRV). TRV equipped with sensors records data that requires a fast algorithm to transform data into helpful information. In all cases, PSD is the appropriate mathematical expression that concludes the track irregularity [5]. The latter aspect of the subject involves some methods to generate the track model at a specific level of required irregularity understudying. The main approaches to developing random rail irregularities are either time integration [6] or spatial integration methods [7]. A transfer function that relates the frequency domain of an irregularity to a white noise signal with constant PSD can be derived directly from a determined PSD function. After applying the appropriate integral transform, they obtained differential equations to be integrated numerically. The other approach employs a discrete-time method using a state-space transition matrix. The derived transfer function is the shape filter whose frequency response magnitude squared matches the PSD [8].

According to the Weiner-Khinchin theorem, two-sided PSD is the Fourier transform of autocorrelation of a time- domain function [9]. Given the PSD, one can determine the amplitude of the real signals using the application of the Inverse Fourier transform. In the discrete sense, the computation of the Fourier transform can be accomplished by the FFT algorithm, which speeds up the calculation of the integrals greatly. The Fourier transform methods or spectral methods provide an efficient computational tool in an extensive field of science and engineering. Indeed, the vast application is possible due to the FFT algorithm in approximating the integral numerically. This paper applies the FFT algorithm to create irregularity with the provided PSD data format. The method is suitable for transforming measuring data to classify track quality onboard in various classes of tracks in the USA and Europe.

2. DESCRIPTION OF TRACK IRREGULARITIES

Many aspects of rail vehicle study require an analytical representation of the track geometry. The quality of the geometry could be described in vertical (v), alignment (a), cross-level (c), and gage variation (g) [1, 2]. These parameters are expressed in Fig. 1 and mathematically in (1) – (4). Among the irregularity, cross-level and alignment variation strongly influences lateral vibration, whereas the gage controls lateral stability. The other vertical irregularity has little impact on lateral vibration.

$$v = (z_L + z_R)/2 \quad (1)$$

$$a = (y_L + y_R)/2 \quad (2)$$

$$c = (z_L - z_R)/2b \quad (3)$$

$$g = (y_L - y_R)/2 \quad (4)$$

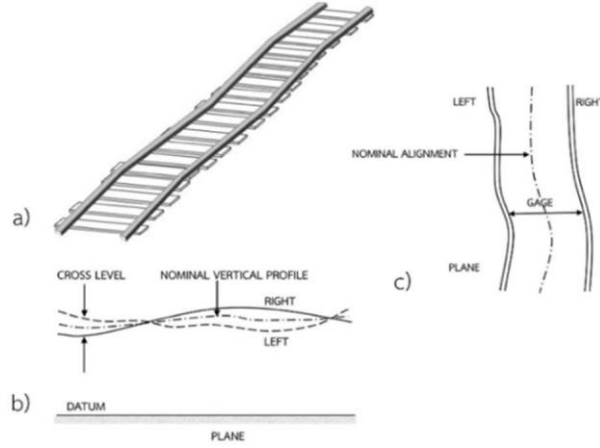


Figure 1 Track irregularity schematic diagram [1]

Due to the random nature of the quantities, PSD in the form of (5) is an appropriate statistical representation of the irregularity [5].

$$S(\Omega) = \frac{A}{\Omega^2} \quad (5)$$

The equations of the PSD described by German high-speed train applications [2] and ORE B176 [10] are expressed for cross-level (S_C), alignment (S_A), and vertical (S_V) irregularity in (6)-(8).

$$S_C(\Omega) = \frac{A_V \Omega_C^2 \Omega^2}{b^2 (\Omega^2 + \Omega_r^2) (\Omega^2 + \Omega_C^2) (\Omega^2 + \Omega_S^2)} \quad (6)$$

$$S_A(\Omega) = \frac{A_A \Omega_A^2}{(\Omega^2 + \Omega_r^2) (\Omega^2 + \Omega_C^2)} \quad (7)$$

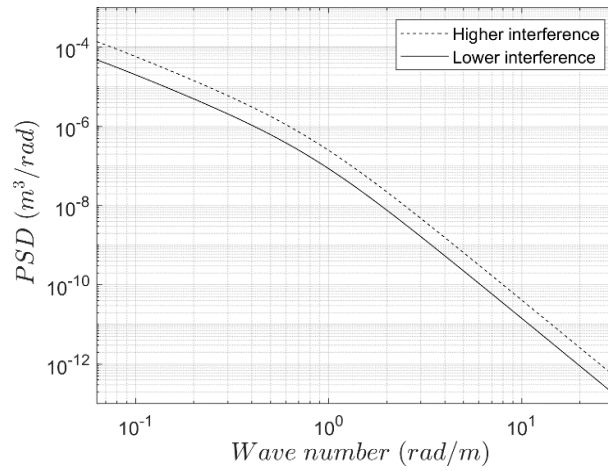
$$S_V(\Omega) = \frac{A_V \Omega_C^2}{(\Omega^2 + \Omega_r^2) (\Omega^2 + \Omega_C^2)} \quad (8)$$

in which $\Omega_C = 0.8246$ rad/m, $\Omega_r = 0.0206$ rad/m, $\Omega_S = 0.4380$ rad/m, and $\Omega_A = 0.8246$ rad/m. The values of A_i are given in TABLE I for the lower and higher interference track classes [2, 11].

Table 1 Track Parameters [2, 11]

A_i	Lower	Higher
A_V (m rad)	4.032×10^{-7}	1.080×10^{-6}
A_A (m rad)	2.119×10^{-7}	6.124×10^{-7}

Fig. 2 shows the PSD of the alignment irregularity analytically obtained from (7) with the provided constants. The recommended wavelength considered in EN13848 to describe the geometric irregularity acceptable levels is in three different ranges of [3, 25], [25, 70], and [70, 200] m. The wavelengths are between 2 to 100 meters for a demonstration to cover all shorter and middle track lengths. This range covers the lowest sampling rate of 0.01 to 0.5 sample/m or the wavenumber (Ω) from 0.0628 to 3.1416 rad/m. However, for the other end of the sampling rate, if any supposed two separated irregular indicators are statistically 0.2 m, the corresponded Nyquist frequency is five samples per meter or 15.57 rad/m. In conclusion, the lowest sampling rate is randomly selected in 0.01 to 0.5 sample/m for each section, whereas the highest sampling rate is more than ten sample/m.

**Figure 2** PSD of the two quality levels of alignment irregularity

3. THE CONTINUOUS REPRESENTATION OF THE PSD

Any track irregularity parameters can be described in a continuous function in the spatial domain as $h(x)$ or in the wavenumber domain as $H(s)$. The two quantities are by mean of the following Fourier transform pair as represented by (9) and (10).

$$H(s) = \int_{-\infty}^{\infty} h(x)e^{2\pi isx} dx \quad (9)$$

$$h(x) = \int_{-\infty}^{\infty} H(s)e^{-2\pi isx} ds \quad (10)$$

In order to get an expression of PSD, we rely on the correlation theorem of $g(x)$ and $h(x)$, which states that Fourier transformation of $corr(h, g)$ is $G(s)H^*(s)$. According to the Wiener-Khinchin theorem, Fourier transformation of the autocorrelation of $h(x)$ is $|H(s)|^2$ or two-sided PSD, $\Phi(s)$.

$$\Phi(s) = \int_{-\infty}^{\infty} corr(h, h)e^{-2\pi isx} dx = |H(s)|^2 \quad (11)$$

A one-sided PSD or $S(s)$ is defined in (12).

$$S(s) = \begin{cases} \Phi(0), & \text{if } s = 0 \\ 2\Phi(s), & \text{if } s \neq 0 \end{cases} \quad (12)$$

4. DISCRETE REPRESENTATION OF PSD IN A FINITE LENGTH

In a discrete form of $h(x)$, the signal values are sampled evenly every interval Δ in (13). For a finite length, L is equal to $N\Delta$ in which N is an integer and the power of 2. For a N consecutive samples, a discrete approximation of (9) is (14).

$$h_n = h(x_n) = h(n\Delta); n = 1, 2, 3, \dots, N - 1 \quad (13)$$

$$H(s_k) = \Delta \sum_{n=0}^{N-1} h_n e^{2\pi i k n / N} \quad (14)$$

in which $s_n = \frac{n}{N\Delta}$, $n = -\frac{N}{2}, \dots, \frac{N}{2} - 1$. We can ignore the scale factor Δ . It is only considered when we need to interpret the result in a physical interval in space. As a result, the formula for the discrete Fourier transform for a set of pair of N samples becomes

$$H_k = \sum_{n=0}^{N-1} h_n e^{2\pi i k n / N} \quad (15)$$

$$h_n = \frac{1}{N} \sum_{k=0}^{N-1} H_k e^{-2\pi i k n / N} \quad (16)$$

A relevant total power to our application is the mean squared amplitude (σ^2), i.e.

$$\begin{aligned} \sigma^2 &= \frac{1}{L} \int_0^L |h(x)|^2 dx \approx \frac{1}{N} \sum_{n=0}^{N-1} |h_n|^2 \\ &= \frac{1}{N^2} \sum_{k=0}^{N-1} |H_k|^2 = \frac{1}{N^2} \sum_{k=0}^{N/2} S_k \end{aligned} \quad (17)$$

As a result,

$$S_k = \frac{1}{N^2} \begin{cases} |H_0|^2 \\ |H_k|^2 + |H_{N-k}|^2, & k = 1, 2, \dots, \left(\frac{N}{2} - 1\right) \\ 2|H_{N/2}|^2 \end{cases} \quad (18)$$

6

5. DFT SYNTHESIS METHOD FOR ALIGNMENT IRREGULARITY

Given the power spectral density either from track measurement system or track classification spectrum, a selection of S_k in the discrete sense should represent $S(\Omega_k)$ for the equivalent power of the bin covering the wavenumber range of $\Delta\Omega = 2\pi/L$. Consequently, S_k is calculated in the integral form over the window function centered of its $S(s_k)$.

$$S(\Omega_k) = S_k = 2\Phi(\Omega_k) \approx \frac{1}{\Delta\Omega} \int_{\Omega_k - \frac{\Delta\Omega}{2}}^{\Omega_k + \frac{\Delta\Omega}{2}} S(\Omega) d\Omega \quad (19)$$

in which $k = 1, \dots, N/2$. We assume that the total power of the signal is zero; thus, $\int_{-\infty}^{\infty} a(x) dx = 0$ or $S(s_0) = S_0 = 0$. The magnitude of a discrete quantity in two-sided PSD can be derived directly from S_k as

$$|H_k| = \sqrt{\frac{1}{2} S_k}, \quad k = 0, \dots, N/2 \quad (20)$$

Since h_n is a real signal, this leads to $H_{-k} = H_k^*$. To create a set of stochastic data from the one-sided PSD, a random phase angle set, φ_k , of $N/2$ data is generated and substituted into (21), by which we can generate the signal for the whole wavelength range $k = 0, 1, 2, \dots, N/2$.

$$H_k = |H_k|(\cos(\varphi_k) + i \sin(\varphi_k)) \quad (21)$$

A spatial signal, h_n is generated after we apply the Inverse FFT algorithm to (21).

6. DESCRIPTION OF THE PROCEDURE FOR ALIGNMENT IRREGULARITY

The section presents the approach to synthesize the track alignment PSD given by the German high-speed railway description. The total energy can be determined from (17), of which the square root is the standard deviation corresponding to the track quality level stated in Table II. The interchange of the irregularity expression in Germany and the USA to be qualified as UIC518 become possible by finding a scale factor A_{QN} from (22) given $S_{qn_k} = A_{QN} S_k$ by substitute (20) in (17)

$$A_{QN} = (\sigma_{QN} / \sigma_{ref})^2 \quad (22)$$

in which $\sigma_{ref} = \frac{1}{N} \sqrt{\sum_{k=0}^{N/2} S_k}$ and σ_{QN} is given in [4]

The development of the process is described by stating the total track length L_{total} having p section, each of which has a constant length L_i and $L_{total} = \sum_{i=1}^p L_i$

$$L_{total} = \{L_1 L_2 L_3 \dots L_p\} \quad (23)$$

L_i is also divided into k sections; thus, $L_i = \sum_{j=1}^k l_{mj}$

$$L_i = \{l_{m_1} l_{m_2} l_{m_3} \dots l_{m_k}\}, \quad l_{m_j} \in [l_{m_{min}}, l_{m_{max}}] \quad (24)$$

in which lm_1 to lm_{k-1} have a random length except lm_k is determined by the remaining length. Each section has its own sample length (sa_i) and quality level (qn_i)

$$sa_i = \{sl_1 sl_2 sl_3 \dots sl_k\}_i, sl_j \in [sl_{min}, sl_{max}] \quad (25)$$

$$qn_i = \{\sigma_1 \sigma_2 \sigma_3 \dots \sigma_k\}_i, \sigma_j \in [\sigma_{min}, \sigma_{max}] \quad (26)$$

After setting up the requirement, we have a restriction for each lm_k to be sampled by N data to be the power of 2. This can be implemented by $m_j = \text{ceil}(\log_2(lm_j/sl_j))$ and $N_j = 2^{m_j}$. Equation (25) is revised by the expression, $sl_j = lm_j/sl_j$. The algorithm for each section lm_j for alignment is as follows

For $j = 1$ to k

$$m = \text{ceil}(\log_2(lm_j/sl_j))$$

$$N = 2^m$$

$$sl_j = \frac{lm_j}{N}$$

$$xsub_j = \frac{lm_j}{N} \{0 \ 1 \ 2 \ \dots \ N - 1\}$$

$$\omega sub_j = \frac{2\pi}{lm_j} \{0 \ 1 \ 2 \ \dots \ N/2\}$$

$$\Omega_l = \omega sub_{jl}$$

$$S = \left\{ S_0 \ S_1 \ S_2 \ \dots \ S_{\frac{N}{2}} \right\}$$

$$S_l = \begin{cases} 0; & l = 0 \\ S(\Omega_l) = \frac{A\Omega_2^2(\Omega_l^2 + \Omega_1^2)}{\Omega_l^4(\Omega_l^2 + \Omega_2^2)}; & l = 1, 2, \dots, \frac{N}{2} \end{cases}$$

$$\sigma_{ref} = \frac{1}{N} \sqrt{\sum_{k=0}^{\frac{N}{2}} S_k}$$

Generate a random phase angle (Uniform distribution)

$$\varphi = \left\{ \varphi_1 \ \varphi_2 \ \dots \ \varphi_{\frac{N}{2}} \right\}, \varphi_l \in [0, 2\pi)$$

Generate stochastic wave length complex number

$$A = \{A_0 \ A_1 \ A_2 \ \dots \ A_{N-1}\},$$

$$A_l = \begin{cases} 0, & l = 0 \\ \sqrt{\frac{1}{2}} S_l e^{-i\varphi_l x}, & l = 1, 2, \dots, \frac{N}{2} \\ \sqrt{\frac{1}{2}} S_{N-l} e^{-i\varphi_{N-l} x}, & l = \frac{N}{2} + 1, \dots, N - 1 \end{cases}$$

8

Generate a random number a_{QN} (Normal distribution)

$$asub_j = a_{QN} IFFT[A]$$

end

Our algorithm can specify the separation error length and section length. In this demonstration, we set the sample length to be less than 0.1 m to capture the minimum separated errors at 0.2 m and random section length between 2 to 100 m. The section length is uniformly selected except for the last one, which has a restriction to complete the total length and is greater than the minimum section range. Nevertheless, our Matlab scripts can change the section length range according to EN13848. Once the above algorithm is implemented for lower interference track quality, the algorithm has been verified by comparing the back-calculated one-sided PSD of each section to their original data in Fig. 2.

A pseudo-stochastic function is quickly introduced by randomly choosing a_{QN} with a provided normal distribution. We set the mean equal to σ_{QN}/σ_{ref} and the standard deviation is equal to 5% of the mean. For demonstration, five km-length tracks with different alignment qualities of QN1 and QN2 are generated according to the German PSD function. The standard deviation at $80 < V \leq 120$ km/h is 1.20 mm for QN1 and 1.50 mm for QN2 [4]. An additional parameter of the track is the range of the irregularity wavelength of [2, 100] m and sample length of 0.2 m. There are 359 track sections within the wavelength range. A cut-off 500 m-length of the generated track is shown in Fig. 3. From (2) and (4), we are then able to synthesize the lateral displacement of the right/left rail for further study in the field of railway vehicle dynamics.

To verify the algorithm, we use (17) to evaluate σ of each section. There are 359 sections for the generated 5-km test track. Fig. 4 shows that the distribution matches the Normal distribution in which the average value complies with the requirement of track quality QN1 at 1.2 mm and QN2 at 1.5 mm. This verifies our algorithm to generate track irregularity at a required track quality.

7. CONCLUSION

The Discrete Fourier Transformation representation of the random irregularity offers an attractive computational form to be implemented using the Fast Fourier Transform algorithm. In addition, the parameters involved can be interpreted in various track quality requirements that relate to the method used to measure the track digitally. The track wavelength stated in EN13848 is the lowest sampling frequency, while the standard deviation stated in UIC518 is interpreted as the root mean square of the amplitude of the irregularity. The irregularity synthesized by the algorithm has the flexibility to conform with both UIC518 and EN13848 upon the given PSDs. This work has to be implemented to further study the influence of the irregularity on railway vehicles dynamics and the track quality measuring system verification.

8. ACKNOWLEDGMENT

This work (P1950662) is supported by Research Development Innovation Management for National Strategic and Network Division, National Science and Technology Development Agency, Thailand.

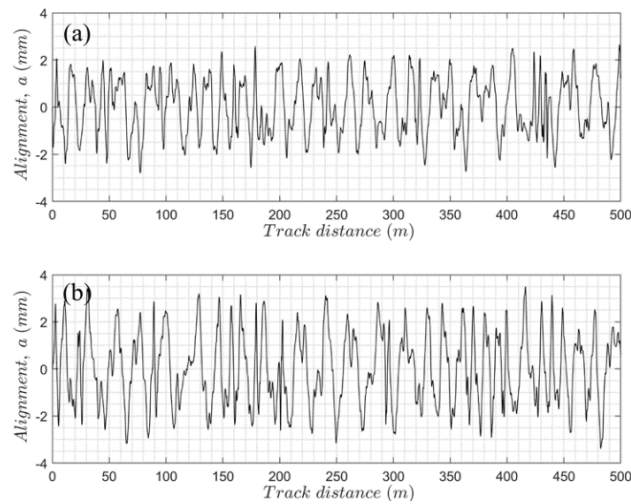


Figure 3 The track alignment synthesis: (a) track quality level QN1
(b) track quality level QN2

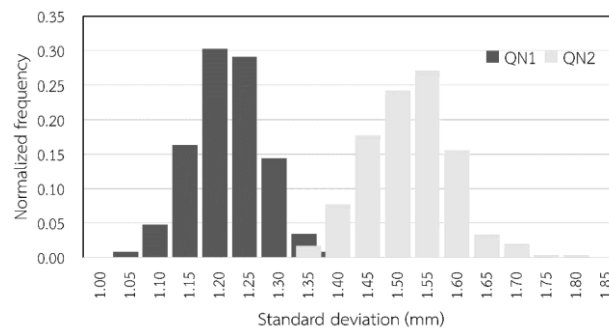


Figure 4 The standard deviation distribution of the generated track for classes QN1 and QN2

9. REFERENCES

- [1] V.K. Garg and R.V. Dukkipat, "Dynamics of Railway Vehicle Systems." 1984, Ontario: Academic Press Canada.
- [2] P. Meinke and A. Mielcarek, "Design and evaluation of trucks for High-Speed wheel/rail application," in Dynamics of High-Speed Vehicles, W.O. Schiehlen, Editor. 1982, SPRINGER-VERLAG.
- [3] A. Hamid and T.L. Yang, "Analytical descriptions of Track Geometry Variations." 1983, FRA-ORD-83-03.
- [4] UIC 518, "Testing and approval of railway vehicles from the point of view of their dynamic behavior-Safety-Track Fatigue-Ride Quality." 2009.
- [5] J.C. Corbin and W.M. Kaufman, "Classifying Track by Power Spectral Density." Mechanics of Transportation Suspension Systems, ASME AMD, 1975. 15: p. 1-20.
- [6] R.C. White, D.A. Limbert, J.K. Hedrick and N.K. Cooperrider, "Guideway-Suspension Tradeoffs in Rail Vehicle Systems," in Arizona State University Engineering Research Center Report. 1978.
- [7] J.E. Dzielski and J.K. Hedrick, "Energy Dissipation Due to Vehicle/Track Interaction." Vehicle System Dynamics, 1984. 13: p. 315-337.
- [8] R.H. Fries and B.M. Coffey, "A state-space approach to synthesis of random vertical and cross-level rail irregularity." Journal of Dynamic System, Measurement, and Control, 1990. 112: p. 83-87.
- [9] W.H. Press, S.A. Teukolsky, W.T. Vetterling and B.P. Flannery, "Numerical Recipes in Fortran 77: The Art of Sceintific Computing." 2nd ed. 2001.
- [10] ORE B 176, "Bogies with steered or steering wheelsets, Report No. 1: Specifications and preliminary studies. Vol. 2. Specification fr a bogie with improved curving characteristics." 1989.
- [11] M. Dumitriu, "Numerical synthesis of the track alignment and application. Part I: The synthesis method." Transport problems, 2016. 11(1): p. 19-28.

**Eco-Efficiency of Smart Reclaimed water management
system: A case study of wastewater treatment from natural
rubber processing
(Condom Production)**

**Phisuttinee Poolchantakorn¹, Jakkapong Chupayak¹, Brian Youichi Kempimook¹,
Preecha Supina¹, Oumaporn Tesiri¹, Surachai Wongcharee², Torpong Kreetachart³,
Supatta Chueycham⁴, Taddao Pahasup-anan⁴, Kowit Suwannahong⁴,**

*¹Thai Nippon Rubber Industry Public Company Limited Si Racha District, Chon Buri,
20110, Thailand*

*²Department of Environmental Engineering, Faculty of Engineering, Mahasarakham
University, Mahasarakham, 44150, Thailand*

*³Department of Environmental Engineering, School of Energy and Environment,
University of Phayao, Phayao, 56000, Thailand*

*⁴Department of Environmental Health Faculty of Public Health Burapha University Chon
Buri, 20131, Thailand*

*E-mail address: Phisuttinee_p@tnrcondom.com, Jakkapong_c@tnrcondom.com,
Brian_k@tnrcondom.com, pth-energy@tnrcondom.com, pth-envi@tnrcondom.com,
surachai.wongcharee@outlook.com, torpong.kr@up.ac.th, benzoic1991@gmail.com,
taddao.pa@go.buu.ac.th, kowit.su@go.buu.ac.th*

Abstract.

The reuse of wastewater reuse has been hailed as a possible alternative solution to cope with the global water scarcity. Reclaimed wastewater may be used to restore the natural water bodies, maintaining the water quality while being environmentally friendly. Industries are demanding a higher quantity of water, which at the same time produces waste. Thailand is a major exporter in the world natural rubber latex production, it has been ability for rubber industries to seek appropriate measures for producing environmentally friendly rubber products. This research aims to study the possibility of reusing the wastewater from production and process in the condom factory through a wastewater treatment system and recycle the water using an IoT with a reverse osmosis method for zero discharge. The result of the study showed promise by lessening the environmental impact and decreasing the operation cost for water treatment. The financial analysis of the RO system was calculated

to have a discount rate of 20.99% with a NPV of 679,759 THB/annum while having a discount payback period of 27 months, indicating that the project was feasible to invest. The ecoefficiency of the project was measured to be 1.47.

This can be a promising strategy but inherently associated operation and maintenance costs need to be considered to fully assess their potential cost-effectiveness.

Keywords. wastewater, IoT, Condom Production, RO system, Reclaimed water

1. INTRODUCTION

The Eastern Economic Corridor (EEC) development project is an extension of the success of the Eastern Seaboard under the Thailand 4.0 strategic plan. Thailand's great leap forward in the industrialization of new s-curve. Clean water and sanitation is the sixth item listed in United Nations Sustainable Development Goals with implementation of circular economic principles within the water sector a widely regarded approach to achieve this goal [1]. Goal 6. 3 specifically addresses the target to increase wastewater recycling and safe reuse. The 3Rs (reduce, reuse, recycle) of waste management are apprehensively analyzed for obtain recommendations and successful implementation of Circular Economy (CE) in the water sector.

Water reuse has become an effective economic solution to tackle the environmental issues for industries. Reusing effluents improves the industry' s image in terms of environmental impact and also reduces cost for the company as less treated water is purchased and there is less reliance on local water sanitation companies. Industrial water reuse and recycling is the process by which wastewater produced from one source is treated to be reused in the same process or recycled for another difference is effective in permeation through a membrane [2]. Opportunities for wastewater reuse and recycling in a natural rubber latex condom manufacturer plant includes a water management system to treat the effluent waste water. It has been demonstrated that a transmembrane pressure difference is effective in permeation through a membrane [3]. For a highly porous membrane with large pore size, the pressure required is lower than for a nanoporous or dense membrane such as the following structure (1) Reverse Osmosis) (2) Nanofiltration (3) Ultrafiltration and (4) Microfiltration [4].

Thailand is currently the world's largest natural rubber producer in the world. As the global leader in natural rubber latex production, it has been a challenge for rubber industries to implement appropriate measures to manufacture environmentally friendly rubber products. Condoms manufactured in Thailand are exported worldwide to many international markets such as China, United States, and Europe. Majority of condoms are made from natural rubber latex (NR condom), with some alternative non-latex synthetic condoms for people allergic to the natural latex protein [5]. The process for manufacturing both NR condom and synthetic condom are similar and follows the steps below; (Fig. 1.) [6].

Incoming materials: the primary raw material used in the production is rubber, which the company employs 60% latex as the main ingredient.

Compound latex: The latex will be homogenized with chemicals into a prevulcanized compound latex and allowed to mature to the appropriate swelling index to obtain a proportionate latex used to produce each type of condom.

Dipping: Starch and dried in a dryer.

Visual inspection: Primarily, our well-trained staff will visually screen the products by checking the condition of the condoms, such as leaks, the edges of the condom, unmatched color, etc.

Electronic testing: Arrange a capacitive hole tester for our testing to meet international standards.

Foil & Packing: The condom is foiled into individual package and packed into consumer boxes as per customer.

Quality Assurance, Quality Control (QA/QC): focused on identifying quality issues in manufactured products.



Figure 1 Process of condom production.

Reclaiming water is an effective option for reducing environmental impact on the world by saving scarce water resources available through reuse of water treatment effluent.

Nowadays, research and practice in the digitalization of the water sector to create a smart water system: IoT (Internet of Things) is a flexible solution designed for the water utility industry, allowing for smarter decisions while optimizing the use of existing resources and investments. Interoperability is one of the key aspects of the IoT that contribute to its growing popularity. Connected or “smart” devices — as “things” in the IoT are often called — have the ability to gather and share data from their environments with other devices and networks. Thus, they need a special method to classify and recycle. In order to address these issues, we implemented the IoT for a wastewater managing system, which detects pollutants mixed in water using IoT and processed in the wastewater treatment into recycled water for reuse. The aim of this research is to study the possibility of reuse of the wastewater after processing the natural rubber processing (condom production) through the wastewater treatment system.

14

Many industries are concerned over the cost to comply with the stringent regulations set by industrialized nations over water quality. In order to tackle this issue, effective water treatment methods through the use of the latest trends, treatment technique, and alternative treatment technology is required to drive cost down for water treatment while providing quality water.

The activities to provide water and wastewater services result which harm to the health of people and the environment. Therefore, reducing water costs and moving to a sustainable water cycle, is a priority for water utilities. This study used ecoefficiency to analyze the effectiveness of the water utilities. Eco-efficiency is defined as the creation of more goods (outputs) and services with fewer resources (inputs) and a smaller environmental impact.

2. METHOD

There are steps, as follows (Fig 2): 1) as a first step to finding the design, 2) Installation process 3) Implementary of research, and 4) evaluation of research that has developed and analyze methods. The wastewater reuse system is presented in Figs. 3 and 4. Fig. 3 shows the process flow chart of the condom production wastewater reuse system, and Fig. 4 shows the point of sensor and meter controlled by IoT.



Figure 2 Step of case study method.

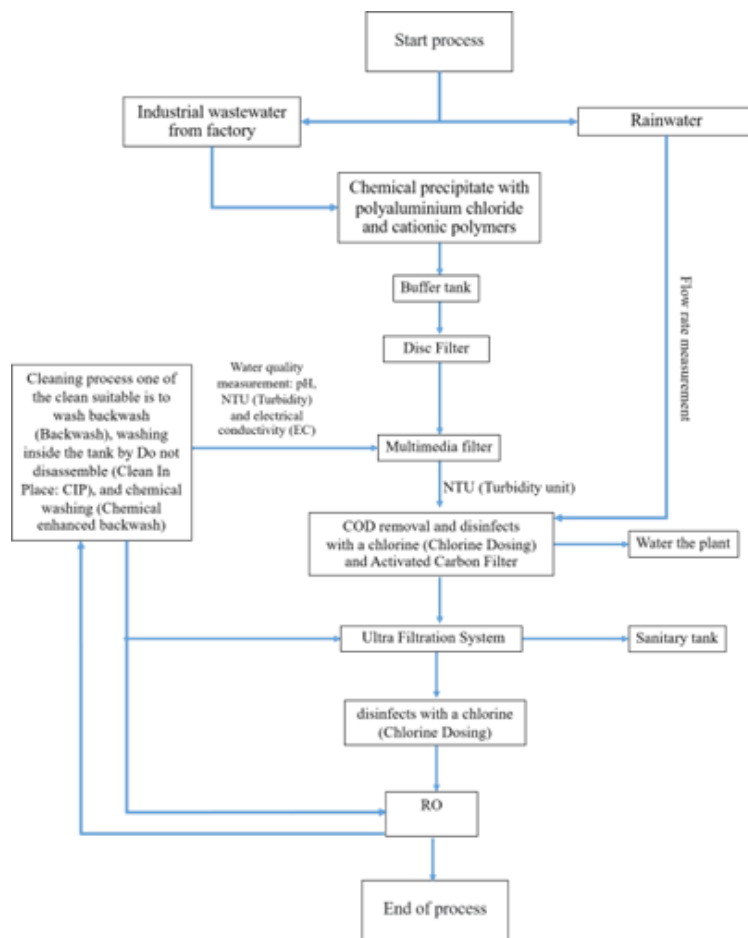


Figure 3 Process Flow Chart – Wastewater treatment

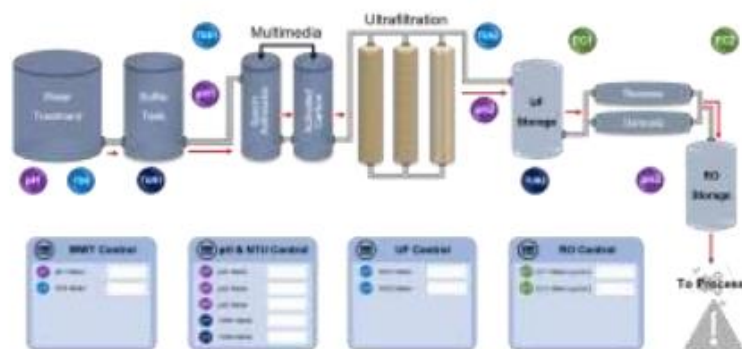


Figure 4 Point of sensor and meter for measuring water quality with IoT real-time monitoring

2.1 Ultrafiltration (UF) System

A pretreatment system is a pre- filtration system designed to remove turbidity, sediment, suspended solids and other compounds such as Chlorine and organic substances that are harmful to the UF system or can result in the UF system not working properly.

It is a tube- type membrane filter cartridge that combines several tubes to trap sediment before use. It has the structure of the rewinding tank made of plastic There are pipes to use on 3 sides, with the top being the bile duct or Permeate, and the sides will have two sides. On one side is the water pipe into the system. On the other side is a water pipe or sewage. There is a filter that used a membrane with a size of 0.1-0.3 microns inside the cylinder. To filter sediment and impurities in the water. (Fig. 5)

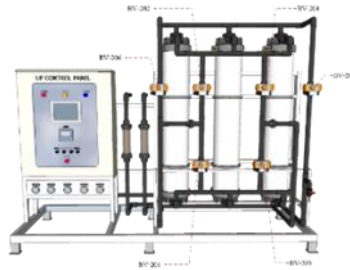


Figure 5 Ultrafiltration (UF) System

2.2 Reverse Osmosis System

The feed water will be pumped from the water storage tank into the system through a series of filters starting with the 5 μ m sediment filter. Afterward, the water is filtered through a membrane filter, which separated the clean water into the RO tank and concentrated water which is directed to the waste collection tank for recycling. The feed water value is measured using the feed conductivity meter and the permeated conductivity smart meter with IoT device gets real-time water consumption (Fig. 6-7).

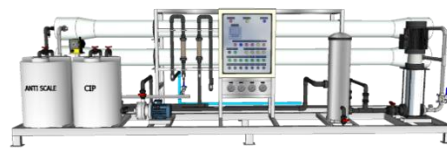


Figure 6 Reverse Osmosis System

CIP for RO system will be done in case of high Concentrate Flow and low permeate flow or in case of inlet-outlet pressure of 5 microns filters having unequal pressure.



Figure 7 Ultrafiltration and Reverse Osmosis System

2.3 Eco-efficiency analysis

Eco-efficiency refers to the ability of firms, industries, regions, or economies to produce more goods and services with fewer impacts on the environment and less consumption of natural resources. It is measured as a ratio of useful outputs (products and services) to environmental inputs (e.g., water consumption and energy consumption) or undesirable environmental outputs. For our study, eco-efficiency was defined as follows: [7]

$$\text{Eco-efficiency} = \frac{\text{Economic performance}}{\text{Environmental impacts}}$$

2.4 Discounted Payback Period: DPB

The discounted payback period (DPB) is calculated from the conversion of accumulated future cash flows received in the future to the present value before calculating from the equation [8].

$$5\text{DPB} = \text{Amount before the payback period} + (\text{Unrefunded portion} / \text{Cash flow incurred in the year of payback})$$

3. RESULT AND DISCUSSION

3.1 Control of the wastewater treatment system, chemical quantity, and origin of wastewater.

Wastewater from the production process has a total flow rate of 100 cubic meters per day. The wastewater is contaminated with natural latex, chemicals used in the latex mixing process, chemicals in the cleaning of latex tanks, various machines and containers. The wastewater is treated by a combination of sedimentation and chemical treatment through the coagulation-flocculation method with aluminum sulfate and cationic polymers. At the end of the wastewater treatment, the treated water is analyzed to ensure that the pH is within the range of 7 ± 0.5 , the COD value not greater than 300 mg/ L and the total dissolved solid value (TDS) not exceeding 2,000 mg/L. The treated water conformed to the specification with the TDS value measuring to be 200 mg/L.

3.2 Production Processes and Water Balance

General water balance of the factory is illustrated in Figure 8. Annually 113,983 m³/day of water input is required, approximately 64,175.23 m³/day of production processes, 49,807.77 m³/day water resource for consumption, 6,060.98 m³/day of condensate for water

reuse. 22,797.00 m³ /day (20%) of water in production processes. The water source is well water which have been subjected to softening. Part of the softened water (102,755 m³ /year) is directly used in the processes while the other portion (142,075 m³ /year) is passed through a reverse osmosis unit to obtain the required water quality for certain production processes.

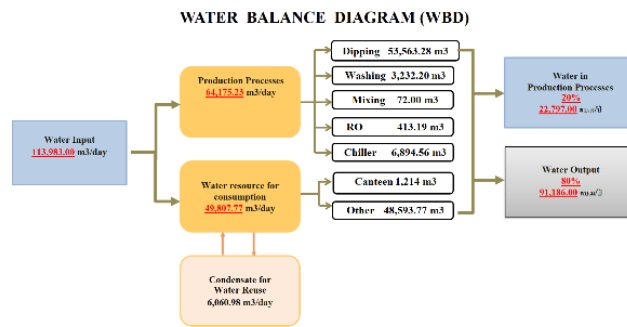


Figure 8 Water balance diagram

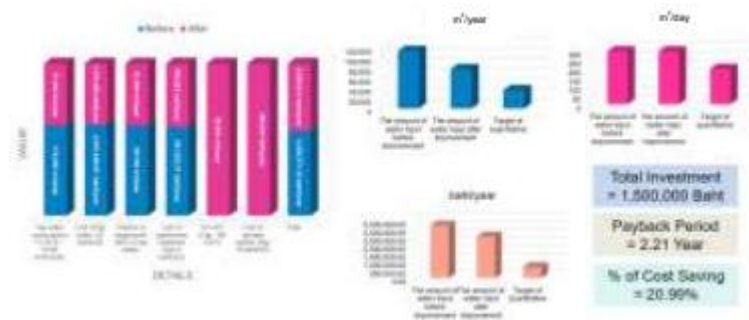


Figure 9 Financial analysis of smart reclaimed water management system

3.3 Financial analysis

A preliminary financial analysis showed the feasibility of the proposed system. The discount rate was calculated to be 20.99% with a NPV of 679,759 baht per year. The discount payback period is 2 years and 3 months, indicating that the project is feasible to invest. (Fig. 9.). This concept's utility is illustrated in the article.

The capital costs for recently completed smart reclaimed water were also reviewed to validate the cost curve. Water is also used in many large scale industrial processes, hotspot of water consumption in the factory as presented in Fig. 10.

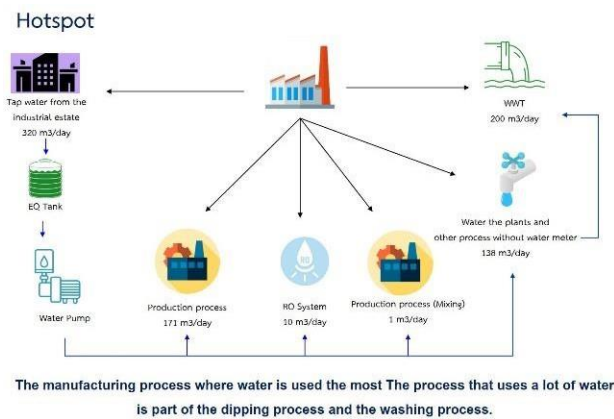


Figure 10 Hotspot: water consumption in condom production

3.4 Eco-efficiency

In this study, we analyzed eco-efficiency trends by analyzing the environmental pressure and economic growth from 2019 to 2021 while aiming to find efficient ways of achieving sustainability.

We used clustering and regression techniques to help us understand the eco-efficiency drivers. Our study result showed that we were able to improve the eco-efficiency of our water treatment process in comparison to 2019 with the eco-efficiency value for 2021 being 1.47 (Fig. 11).

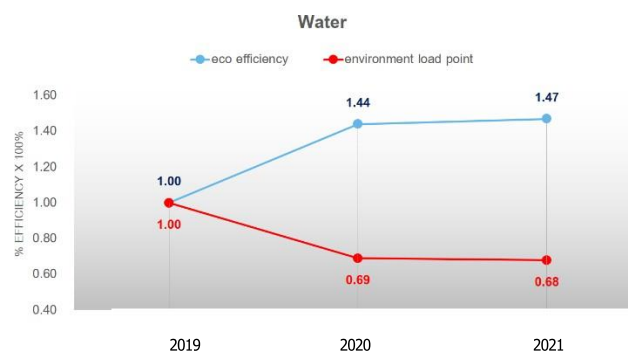


Figure 11 Eco-Efficiency of water reclaimed water

Industrial water quality issues have been addressed in this study through water treatment methods by studying the use of the latest trends, treatment technique, and alternative treatment technology is required to drive cost down for water treatment while providing quality water.

This study analyzes the 2019 – 2021 eco-efficiency trends with the aim to contribute to the sustainable development of the Eco-factory. While eco-efficiency of all of the indicators that we analyzed showed improvements during the study period, a gap remained in comparison to the more advanced eco-efficiency observed both domestically and internationally. Decoupling indices were introduced in order to examine the decoupling

relationship between environmental pressure and economic growth. This analysis demonstrated that some progress occurred during the study period resulting from the implementation of existing policies and measures entailing resource conservation and reduction in the emission of pollutants.

4. CONCLUSION

The present work examined and confirmed the possibility of using membrane technology for effluent treatment from an industrial wastewater treatment plant with the goal for reuse of the treated water through a combination of ultrafiltration followed by reverse osmosis. The study demonstrated the effectiveness of the treatment technologies of the reclaimed water system. The results of the study shows that the proposed smart reclaimed water treatment system is effective for our condom manufacturing plant and has the potential to be applicable for similar industries with similar volume and wastewater contaminants types [9].

5. ACKNOWLEDGMENT

This research was supported from Faculty of Public Health Burapha University, Thailand and Thai Nippon Rubber Industry Public Company Limited.

6. REFERENCES

- [1] B. Van der Bruggen, "Microfiltration, ultrafiltration, nanofiltration, reverse osmosis, and forward osmosis" *Fundamental Modelling of Membrane Systems*, 2018, pp. 25–70.
- [2] K. Suwannahong, S. Wongcharee, J. Kreanuarte, and T. Kreetachart. "Pre-treatment of acetic acid from food processing wastewater using response surface methodology via Fenton oxidation process for sustainable water reuse", *J. sustain. dev. energy water environ. syst.*, 9(4), 1080363.
- [3] S. Alizadeh, H. Zafari klukhi, , F. Rostami, , M. Rouhbakhsh, &, A. Avami, "The eco-efficiency assessment of wastewater treatment plants in the city of Mashhad using emergy and life cycle analyses" *Journal of Cleaner Production*, 2019, 119327.
- [4] P. Irena, K. Jasmina, P. Damijan, H.-N. Claus. "A feasibility study of ultrafiltration /reverse osmosis (UF/RO)-based wastewater treatment and reuse in the metal finishing industry" *Journal of Cleaner Production*, 2015, 101, pp. 292–300.
- [5] R. Ordóñez, D. Hermosilla, I. S. Pío, and Á. Blanco, "Evaluation of MF and UF as pretreatments prior to RO applied to reclaim municipal wastewater for freshwater substitution in a paper mill: A practical experience," *Chemical Engineering Journal*, 2011, 166, pp. 88–98.
- [6] A. Suárez, P. Fernández, J. Ramón Iglesias, E. Iglesias, and F. A. Riera, "Cost assessment of membrane processes: A practical example in the dairy wastewater reclamation by reverse osmosis" *Journal of Membrane Science*, 2015, 493, pp. 389–402.

- [7] N. Atanasova, M. Dalmau, J.Comas, M.Poch, I.Rodriguez-Roda, and G.Buttiglieri, “Optimized MBR for greywater reuse systems in hotel facilities ” *Journal of Environmental Management*, 2017, 193, pp . 503– 511.
- [8] A. Marchioni and C. A. Magni, “Investment decisions and sensitivity analysis: NPV-consistency of rates of return” *European Journal of Operational Research*, 2018, 268, pp. 361–372.
- [9] I. Petrinic, J. Korenak, D. Povodnik, and C. Hélix-Nielsen, “A feasibility study of ultrafiltration/reverse osmosis (UF/RO)-based wastewater treatment and reuse in the metal finishing industry,”*Journal of Cleaner Production*, 2015, 101, pp. 292–300.

Drying of Unripe Banana (*Musa sapientum* Linn.) Using Microwave Combined with Hot Air

Nattapol Poomsa-ad¹, Lamul Wiset²

¹Drying Technology Research Unit, Faculty of Engineering Mahasarakham University
Maha Sarakham, Thailand

²Postharvest Technology and Agricultural Machinery Research Unit, Faculty of
Engineering Mahasarakham University Maha Sarakham, Thailand

E-mail address: nattapol.p@msu.ac.th¹, lamulwiset@hotmail.com²

Abstract.

The objective of this research is to study the effect of microwave power on the quality of dried unripe banana including energy consumption. The microwave power was varied from 0-2,000 watts combined with drying temperature of 50 °C. The sliced of unripe banana with the thickness of 3 mm was used. Sample was dried until the a_w was lower than 0.6. Then, color values in term of $L^* a^* b^*$, whiteness index and viscosity was determined. Result was found that the trend of L^* value was decreased when microwave power increased. In addition, the viscosity was the highest when using the microwave power at 1,000 watts. Moreover, the increase in microwave power resulted in the decrease in energy consumption. When considering in quality and energy consumption, the drying at microwave power of 1,000 watts combined with hot air at 50 °C is recommended for unripe banana drying.

Keywords. dehydration, electromagnetic energy, flour.

1. INTRODUCTION

Unripe or green banana (*Musa spp. L.*) is considered as healthy ingredient with a potential source of bioactive compounds and can be used as a functional immunostimulatory food ingredient [1-2]. It contains high resistant starch which is an excellent probiotic growth promotion [3-4]. Volunteers who consumed unripe banana flour for 6 weeks found that significantly reduced hunger and increase satiety with glucose homeostasis in health. This might reduce risks of certain non- communicable diseases owing to its high resistant starch level [5].

Drying is one of important process of green sliced banana into flour. Nowadays, microwave techniques have been applied to reduce moisture content for fruit and food

products. This is due to high drying rate which reduce the drying time as well as energy consumption reduction [6-8]. Apart from considering in energy consumption, quality of product is considered as important variable for consumer and product user in particular texture, appearance, flavor, color and rehydration in some product e.g. mushroom. Products have been dried with microwave assisted hot air drying had acceptable quality [9-12]. Moreover, consumers are interested in bioactive compounds and antioxidant activity. Microwave-hot air drying could maintain these compounds which was better than only hot air drying [13]. Also, there has been reported that phenolic compounds of dried saskatoon berries with microwave vacuum drying was not significantly different with freeze drying [14].

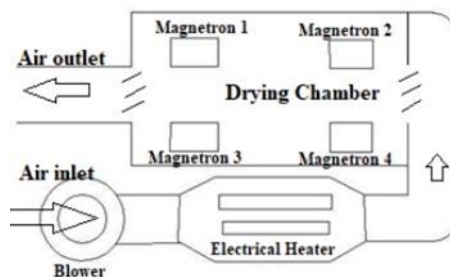
In this work, we are interested in drying unripe banana using microwave assisted hot air. Quality of dried unripe banana and energy consumption of drying are studied to find the suitable microwave power.

2. MATERIAL AND METHOD

2.1. Microwave-hot air dryer



a) The pilot scale microwave assist hot air dryer



b) Schematic of the dryer

Figure 1 Experimental dryer

The pilot scale microwave assist hot air dryer was constructed at Faculty of Engineering, Mahasarakham University, Thailand. A schematic diagram of this dryer is shown in Figure 1. Drying chamber size of this equipment was 80 (L) x 80 (W) x 80 (H) cm and manufactured with stainless steel No. 304. The four of 1000 W magnetrons were used to generate microwave with the frequency of 2,455 MHz. Hot air generator and circulator used 9 kW electric heater and 1.5 kW centrifugal fan with electric motor. Hot air duct was connected to drying chamber with flange and perforated plate was installed for microwave shielding. The circular trays with driving system were mounted to the bottom of the drying chamber. The turning speed was adjusted by using frequency inverter.

2.2. *Sample preparation*

Banana cv. Namwa was purchased from local market in Maha Sarakham province. Banana with green color and unripe stage was only used in this study. It was boiled for 45 second before peeling and then soaked in 1% sodium metabisulfite solution for 30 minute to prevent browning reaction. Then, it was sliced using slicing machine to obtain the sample with thickness of 3 mm. The sliced unripe bananas of 500 g were placed on tray as shown in Figure 2.



Figure 2 Tray sample and arrangement

2.3. *Drying condition*

The microwave power was varied to 0, 500, 1,000, 1,500 and 2,000 watts combined with hot air at drying temperature of 50 °C. Unripe banana was dried until the a_w less than 0.6 to prevent the microbial growth. The drying was conducted for 2 duplications for each treatment. After drying, sample was ground to pass a 45-mesh sieve to obtain homogenous before quality analysis.

2.4. Quality determination

Moisture content

Unripe banana was chopped to small piece before determining moisture content. It was used oven method at temperature of 103 °C for 24 hr. Moisture was calculated from the water evaporation divided by the fresh weight

Water Activity (a_w)

Dried sample was measured the a_w using an AquaLab water activity meter (Aqua-Link 3.0, Pullman, WA) which was calibrated with distilled water to obtain a_w in the range of 1.000 ± 0.003

Color values

The color of sample was measured by a Hunter Lab Colorimeter (type Color Flex, USA). The Hunter L^* , a^* , b^* scale gave measurement of colors in units of approximate visual uniformity throughout the solid. The L^* value measures lightness and varies from 100 for a perfect white and 0 for black, a^* and b^* when positive measure redness and yellowness, respectively. For whiteness index (WI), it was calculated as following

$$WI = 100 - [(100 - L)^2 + (a^2 + b^2)]^{1/2}$$

Viscosity

Unripe flour was mixed with water at the ratio between flour (dry weight) and water of 20:500. Mixing sample was controlled the temperature of hot plate at 30 °C with magnetic stirrer for 15 minute. The solution was measured the viscosity using Brookfield Viscometer Model LVDV-E with the probe number 61. The highest torque was recorded as the obtained viscosity.

Energy consumption

Energy consumption from 3 phases was determined using digital electric meter (brand Easton model sdm 230-8i) with 5% less error. The energy consumption was from different sources i.e. blower, heater, motor and microwave power.

3. RESULTS AND DISCUSSIONS

Table 1 presents the drying time, initial moisture content, final moisture content and a_w of unripe banana drying. You can see that the drying time is decreased when the microwave power increased. This due to the microwave power could accelerate the moisture evaporation from inside to environment. This finding is agreed with the previous report that drying time of using microwave combined with hot air was reduced in particular increasing microwave power [6-8]. The a_w in all treatments was lower than 0.6 which is safe for further process and longer storage.

Table 1 Drying time, moisture content and water activity of unripe banana drying

Microwave power (W)	Drying time (h)	Initial Moisture content (% w.b.)	Final moisture content (% w.b.)	Water Activity a_w
0	6	68.81+0.33	7.99+0.47	0.27+0.02
500	4.5	67.61+0.98	7.49+0.11	0.25+0.03
1000	3	69.19+3.13	6.86+1.40	0.25+0.07
1500	2	67.84+1.08	6.92+0.76	0.22+0.05
2000	1.5	68.36+1.03	7.98+0.40	0.30+0.07

After drying, the product was ground to become homogenous before measuring the color. The color values are shown in Table 2. The significant result is L^* value. The L^* value represents the brightness, the product from the study is brighter than the product purchased from the market. This might be the drying method was different which caused the different color. However, the increase in microwave power results in the decrease in brightness and increase in redness (a^*). This might be the browning reaction occurred when increased microwave power. In overall appearance, the whiteness index is used to assess the color quality. It is found that all treatments show significant higher than commercial product. This could be implied that the drying by microwave combined with hot air drying is good in color assessment. However, by visual evaluation, the picture of product is shown in Figure 3. It is illustrated that all products are similar appearance.

Table 2 The color values and whiteness index of dried unripe banana

Microwave power (W)	L^*	a^*	b^{*ns}	Whiteness index
Commercial product	84.42±0.37 ^d	2.05±0.01 ^a	10.41±0.06	80.98±0.27 ^c
0	90.41+0.34 ^a	0.11+0.07 ^c	10.80+0.95	85.55+0.94 ^a
500	90.51+0.12 ^a	0.16+0.27 ^c	10.92+0.70	85.53+0.61 ^a
1,000	88.72+1.79 ^{bc}	0.63+0.51 ^b	11.89+1.73	83.59+2.50 ^b
1,500	89.74+0.50 ^{ab}	0.13+0.08 ^c	10.91+0.97	85.02+1.05 ^{ab}
2,000	88.45+0.63 ^c	0.51+0.52 ^{bc}	11.30+0.33	83.85+0.70 ^{ab}

ns=non significance different

Means with the different letter within a column are significantly different ($p \leq 0.05$) by DMRT



Figure 3 Dried product from different microwave power combined with hot air at 50 °C

Viscosity is one of an important factor of power to be considered for further use in ingredient mixing with other components to make the product. If the viscosity is still high, it means that the property of flour is still good for using as ingredients. It is implied that the longer drying time and higher heat cause the disruption of internal structure of product. The drying at 1,000 watts had the best viscosity in this study with the drying time only 3 hr. Also, the viscosity is higher than the product from the market.

Table 3 The viscosity of solution prepared from dried unripe banana

Microwave power (W)	Viscosity (cP)
Commercial product	21.31±0.94 ^b
0	15.29±1.77 ^{de}
500	18.90±3.58 ^{bc}
1,000	24.59±2.05 ^a
1,500	17.51±3.43 ^{cd}
2,000	14.10±0.54 ^e

Means with the different letter within a column are significantly different ($p \leq 0.05$) by DMRT

You can see that the total energy consumption is considered from different sources i.e. blower, motor, heater and microwave. The highest energy consumption is from heater. This is the reason why drying without microwave has the highest energy consumption. Therefore, the increase in microwave power results in the less energy consumption. Therefore, to produce the dried product, the producers have to consider in the quality as well as the energy consumption. In this study, when consider in quality and energy use, the drying at 1,000 watts combined with hot air is appropriate

This finding is an alternative process for potential producer. With this method we could control product with good quality. However, the only 500 g sample was used in this research. Therefore, scale up process is necessary for mass production. Considering in energy consumption, we can replace heater by using LPG to reduce the processing cost

Table 4 Energy consumption of drying with different conditions

Microwave power (W)	Drying time (h)	E _{blower} (kWh)	E _{motor} (kWh)	E _{heater} (kWh)	E _{microwave} (kWh)	E _{total} (kWh)
0	6	1.41	0.84	15.33	0.00	17.58
500	4.5	1.05	0.63	11.49	2.25	15.43
1,000	3	0.70	0.42	7.66	3.00	11.79
1,500	2	0.47	0.28	5.11	3.00	8.86
2,000	1.5	0.35	0.21	3.83	3.00	7.39

4. CONCLUSION

The unripe banana was dried under different microwave powers assisted with hot air at drying temperature of 50 °C. It could be concluded as following.

- The drying time was decreased from 6 hr without microwave power to 4.5, 3, 2 and 1.5 hr when used microwave power at 500, 1,000, 1,500 and 2,000 watts, respectively.
- The trend of L* value was decreased when the microwave power increased. While as a* value was increased.
- The drying at 1,000 watts had the highest viscosity.
- The increase in microwave power resulted in the decrease in energy consumption.
- When considering in quality and energy consumption, the drying at microwave power of 1,000 watts combined with hot air 50 °C is recommended for unripe banana drying.

5. ACKNOWLEDGMENT

The authors would like to thank Faculty of Engineering, Maharakham University for financial support. Also thanks to Mr. Thanakorn Yothanon for doing experiment

6. REFERENCES

- [1] K. Horie, M. S. Hossain, S. Morita, Y. Kim, A. Yamatsu, Y. Watanabe, and M. Kim, "The potency of a novel fermented unripe banana powder as a functional immunostimulatory food ingredient," *J. Funct. Foods*, vol. 70, 103980, July 2020.
- [2] L. Chang, M. Yang, N. Zhao, F. Xie, P. Zheng, J. Simbo, and S. K. Du, "Structural, physicochemical, antioxidant and in vitro digestibility properties of banana flours from different banana varieties (*Musa spp.*)," *Food Biosci*, vol. 47, 101624, June 2022.
- [3] L. Chang, M. Yang, N. Zhao, F. Xie, P. Zheng, J. Simbo, and S. K. Du, "Structural, physicochemical, antioxidant and in vitro digestibility properties of banana flours from different banana varieties (*Musa spp.*)," *Food Biosci*, vol. 47, 101624, June 2022.
- [4] P. Jaiturong, N. Laosirisathian, B. Sirithunyalug, S. Eitssayeam, S. Sirilun, W. Chaiyana, and J. Sirithunyalug, "Physicochemical and prebiotic properties of resistant starch from *Musa sapientum* Linn., ABB group, cv. Kluai Namwa Luang," *Heliyon*, vol. 6(12), e05789, December 2020.
- [5] F. A. H. Sarda, E. B. Giuntini, M. L. P. Gomez, M. C. Y. Lui, J. A. Negrini, C. C. Tadini, and E. W. Menezes, "Impact of resistant starch from unripe banana flour on hunger, satiety, and glucose homeostasis in healthy volunteers," *J. Funct. Foods*, vol. 24, pp. 63-74, June 2016.
- [6] Q. Guo, D. Sun, J. Cheng, and Z. Han, "Microwave processing techniques and their recent applications in the food industry." *Trends Food Sci Technol*, vol. 67, pp. 236-247, September 2017.
- [7] J. Dehghannya, S. Hosseinlar, and M.K. Heshmati, "Multi-stage continuous and intermittent microwave drying of quince fruit couple with osmotic dehydration and low temperature hot air drying," *Innov Food Sci Emerg Technol*, vol. 45, pp. 132-151, February 2018.
- [8] Y. Wang, X. Li, X. Chen, B. Li, X. Mao, J. Miao, C. Zhao, L. Huang, and W. Gao, "Effects of hot air and microwave-assisted drying on drying kinetics, physicochemical properties, and energy consumption of chrysanthemum," *Chem. Eng. Process*, Vol. 129, pp. 84-94. July 2018.
- [9] A. Nawirska-Olszanska, B. Stepien, and A. Biesiada, "Effectiveness of the fountain-Microwavedrying method in some selected pumpkin cultivars," *LWT - Food Sci Technol*, vol. 77, pp. 276-281, April 2017.
- [10] G. Cuccurullo, L. Giordano, A. Metallo, and L. Cinquanta, "Drying rate control in microwave assisted processing of sliced apples," *Biosyst. Eng.*, vol. 170, pp. 24-30, June 2018.
- [11] Q. Wang, S. Li, X. Han, Y. Ni, D. Zhao, and J. Hao, "Quality evaluation and drying kinetics of shitake mushrooms dried by hot air, infrared and intermittent microwave-assisted drying method," *LWT - Food Sci Technol*, vol. 107, pp. 236-242, June 2019.
- [12] Y. Jia, I. Khalifa, L. Hu, W. Zhu, J. Li, K. Li, and C. Li, "Influence of three different drying techniques on persimmon chips' characteristics: A comparison study among hot-air, combined hot-air-microwave, and vacuum-freeze drying techniques," *Food Bioprod. Process*, vol. 118, pp. 67-76. November 2019.

- [13] E. Horuz, H. Bozkurt, H. Karatas, and M. Maskan, "Effects of hybrid (microwave-convectional) and convectional drying on drying kinetics, total phenolics antioxidant capacity vitamin C, color and rehydration capacity of sour cherries," *Food Chem.*, vol. 230, pp. 295-305. September 2017.
- [14] S. Lachowicz, A. Michalska, K. Lech, J. Majerska, J. Oszmianski, and A. Figiel, "Comparison of the effect of four drying methods on phenols in saskatoo berry," *LWT –Food Sci Techno*, vol. 111, pp. 727-736, August 2019.

Development of Fiber Stripping Machine for Eri Cocoon

Kasorn Wongkasem¹, Surachai Wongcharee¹, Nantawatana Weerayuth³, Pitak Promthaisong¹, Kaned Toong-ood¹

¹Faculty of Engineering Mahasarakham University Mahasarakham, Thailand

²Faculty of Engineering Ubonratchathanee University Ubonratchathanee, Thailand

*E-mail address: kasorn.wong@msu.ac.th, surachai.w@msu.ac.th,
weerayuth_gm@hotmail.com, pitak.p@msu.ac.th, kaned1987@gmail.com*

Abstract.

Eri silk has economic significance. It can make fibers into silk threads which shiny distinct, and unique. Producing silk fibers begins with the silk fiber peeling to prepare for the cutting process and silk carding. Silk stripping is currently stripping by hand. The survey found that it can peel an average of 150 grams per 1 hour. This research aims to create a silk fiber stripping machine from the eri cocoon to increase the rate of fiber stripping. The fiber stripping machine is 70 centimeters wide, 100 centimeters long, and 105 centimeters high. The cocoon conveyor belt is responsible for conveying the eri cocoon to the fiber stripping core. The fiber stripping core is used to peel the fibers that surround the cocoon. A motor is operated to transmit power to the spinning axis. And the cocoon flick core transports the cocoons that have been stripped into the support container. The rate of fiber removal is 1 kilogram of cocoon per hour from the experiments. The results showed that eri silk peeling using a machine could give a 6.66 times better rate of fiber removal than manual peeling. In addition, the development of this fiber peeling machine from this research can increase the rate of fiber removal from the nest, reducing the labor even more. Moreover, the cocoons that were still clean. Therefore, it can increase income for the farmer of silkworm community enterprise.

Keywords. eri, cocoon, fiber, peeling striping, machine.

1. INTRODUCTION

Eri silk has economic significance. The eri cocoon produces fibers surrounded by sericin, a sticky substance that binds the fibers into a silkworm cocoon. Eri cocoon has a long, slender,

white color. The cocoon is relatively flat, with an average width of 2.1 centimeters and an average length of 4 centimeters [1, 2, 3]. Eri fibers are shorter and looser than mulberry silk [4, 5, 6, 7]. Pulling threads from the cocoon uses a spinning method. There are both hand-spinning and machine-spinning. Fiber production begins by taking the eri cocoon to peel off the fiber. Then cut the cocoon to separate the pupa, boil it to degumming, and spin up the yarn. Spun yarn is a raw material that the industry needs a lot. Peeling fibers is essential for cleaning cocoons. In addition, it also separates the black and dirty parts to increase the price cocoons. Removing the silk fibers from the cocoon is similar to today's traditional wisdom. It is peeling by hand, using human labor, which requires a long time to remove silk fibers that can peel an average of only 150 grams per 1 hour. Therefore, the silk fiber peeler will help to prepare the cocoon into the cutter. From various data surveys and study the problems regarding cocoon preparation; accordingly, there is an idea of creating a silk stripping machine that can give the rate of fiber peeling better than fiber peeling by hand [8,9,10,11,12]. Moreover, farmers will get clean cocoons, increase income, and reduce human labor.

2. MATERIALS AND METHOD

The study of data on eri fiber production found that eri silk fiber removal by hand. The outer part of the cocoon has a section called the fiber wrap, causing the cocoons to clump together. Therefore, separating the pupa from the cocoon is difficult. By cutting the cocoon to separate the pupa, farmers need to use their hands to pull off the silk fiber. Therefore, removing fibers from the cocoon is essential in fiber production. The threads can be removed by hand, as shown in Fig. 1. The design of the stripping machine (as shown in Fig. 2) used the characteristics of eri fiber wrapped.

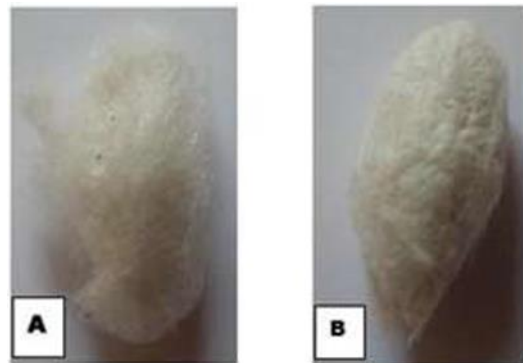


Figure 1 (A) The cocoon before stripping
(B) Cocoon after stripping

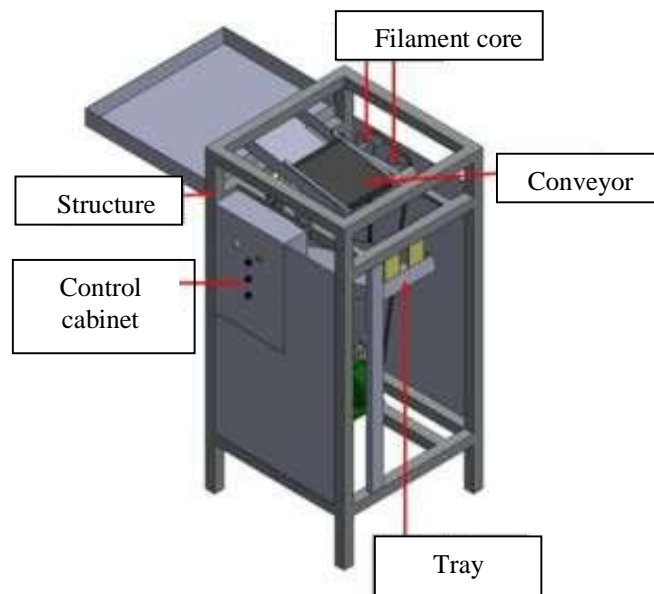


Figure 2 Design of the eri silk fiber stripping machine

The components of the machine are as follows: 1) structure of the device is made of 0.1 cm thick stainless steel. The dimension of the machine is the width of 60 centimeters, length of 60 centimeters, and height of 125 centimeters. The peeling device is covered with a stainless steel sheet on all four sides to increase safety for use. 2) The filament core has a diameter of 1.2 centimeters, 47 cm in length. The core is attached with anti-slip tape wrapped around the core. A gear motor is used to send power to the fiber stripping core. The engine can adjust the speed from 600-2500 rpm, responsible for peeling the silk fiber wrapped outside the cocoon. 3) Conveyor is transmitted by a gear motor. The velocity of the conveyor belt can be adjusted from 17.27 to 69.11 meters per minute. It is responsible for transporting the silkworm cocoon forward to the fiber stripping axis. 4) The control cabinet consists of an on-off switch to adjust the speed. 5) The silkworm trays are then peeled off and served as containers to support the cocoon eri.

3. EXPERIMENTAL DESIGN

In the experiment, to find the efficiency and working rate of the silk peeling machine, results are compared to fiber peeling by hand. Experiments are divided into three parts. In the first part, the speed of the stripping rod is adjusted to 600, 1250, 1800, and 2500 rpm. The second part is the conveyor speed adjusted by 5 rpm, 10 rpm, and 20 rpm. The third part is that the variety of cocoons is changing. There are two types of eri cocoons, 1) fresh eri cocoons. The appearance of the fresh cocoon is a stable, hard shell, with an average weight of 1.85 grams per nest, making it easier to transport on the belt. 2) Dry cocoons in which the outer shell is not hard. The nest will collapse according to the compression of the belt. The experiment will take one hour to remove fibers and check the quality of eri cocoons that have been

stripped. The results are used to find the average rate per hour and the cleanliness of the cocoon.

4. EXPERIMENTAL RESULTS

The eri silk fiber stripping machine is constructed (as shown in Fig. 3) to increase the rate of fiber removal from the nest and reduce human labor. Moreover, it can increase the income of the farmers. The comparison of the fiber stripping rates is shown in Fig.4-6. The rates of peeling by machine are presented in TABLE1. It can be analyzed as follows. The best rate of peeling is 1088.23 grams per hour when the speed of the belt is five revolutions per minute and the speed of the stripping axis 1800 revolutions per minute. On the other hand, the quality of the striated cocoon is 146.71 grams per hour when the belt speed is 20 rpm, and the speed of the fiber stripping core is 1250 rpm. From the experimental table, it can be seen that if the belt speed is too high, peeling fiber will not have good quality. The experiments of peeling the dry cocoons found that the rate of peeling is 18.51 grams per hour. The belt speed is adjusted at 20 revolutions per minute, and the speed of the fiber stripping axis is 2500 revolutions per minute. From the experiment, it can see that the cocoon is dry cocoons are not able to peel the fibers due to their lightweight. The dry cocoon has no hardness and soft appearance, so it is easily compressed. From TABLE 2, it was found that the fiber extract from fresh cocoon has the best efficiency, able to peel 96.1242 grams per hour when using the belt speed of 5 revolutions per minute, the fiber peeling axis speed of 1993. 66 rpm. The minimum peeling rate is 28. 9909 grams per hour. After adjusting the conveyor speed to 20 revolutions per minute and adjusting the revolving speed of the axis at 1610 revolutions per minute, the desirability value is 0.192. The best of the experiment is the machine can peel 28.132 grams per hour when the belt speed is 20 revolutions per minute, peeling axis speed of 2500 rpm. The minimum stripping rate is 4.735 grams per hour when adjusting the conveyor speed at five revolutions per minute and then adjusting the revolving speed of the silk stripping axis at 600 revolutions per minute.

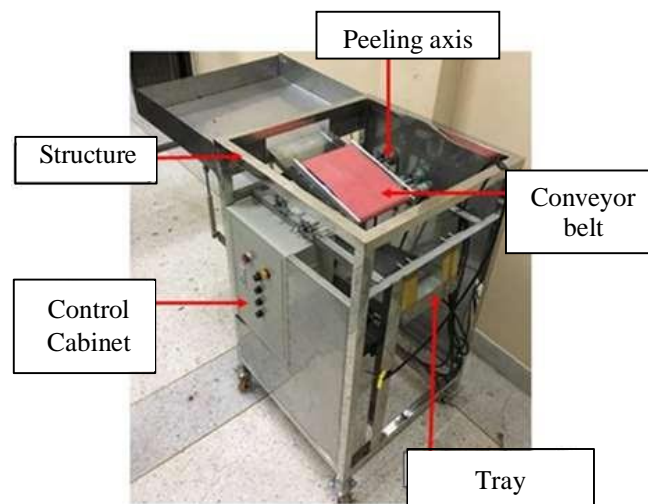


Figure 3 The eri silk fiber stripping machine



Figure 4 Dry cocoon before peeling fibers



Figure 5 Fresh cocoons before peeling fibers



Figure 6 The cocoons completely peel the fibers

Table 1 The results of the rate of peeling

Speed of conveyor (rpm)	Speed of peeling axis (rpm)	Rate of peeling (grams per hour)
5	600	404.7
	1250	944.18
	1800	1088.20
	2500	600.00
10	600	174.95
	1250	274.70
	1800	222.10
	2500	432.38
20	600	200
	1250	146.71
	1800	212.65
	2500	256.98

Table 2 The results of the rate of peeling in the various speed of the peeling axis

Speed of conveyor (rpm)	Speed of peeling axis (rpm)	Rate of peeling (grams per hour)
5	1993.66	962.24
	2015.08	962.19
	2022.13	962.16
	2089.02	960.32
10	1866.72	958.59
	1763.34	950.84
	1538.67	970.20
20	1595.82	28.99
	1610.00	28.99

5. CONCLUSIONS

The test of silk fiber removal by eri machine found that removing the fiber from the machine can give a 6.66 times better rate than the fiber removal by hand. The advantage of this

machine is that it can help solve the problem of cleaning pupae before boiling them for degumming. In addition, the stripped fibers can also use for spinning yarn. The disadvantage is that it is difficult to set the peeling axis distance because Eri cocoons are thin and soft. Therefore, the peel-axis setting must be set to suit the size of the cocoon. In further developments, suitable materials must be found to make the peel core and set the exact distance for the eri cocoon. In addition, it can increase farmers' income, reduce human labor, and obtain a clean eri cocoon.

6. ACKNOWLEDGMENT

The research team would like to thank the Faculty of Engineering, Maharakham University, funded this research. Thank the Center for Excellence in Innovation, Maharakham University, and the Faculty of Engineering, Maharakham University, which provides knowledge, information, and recommendations useful for research.

7. REFERENCES

- [1] Thipwadee, "Eri forest silkworm raising with various food plants". Department of Entomology Faculty of Agriculture, Kasetsart University: Kasetsart University, 2005
- [2] Kobkun, "Research and Development of Pa Eri Silk Silk" in the northeastern region, Department of Agriculture, 2006.
- [3] S. Sivilai, T. Sangtamat, W. Saksiriret, and Waikakul, Y. "New food plants for eri silkworm rearing", In Program and Abstracts of International Workshop on Wild Silkmoths and Silk "Current Advances and Development in Wild Silkmoths and Tropical Bombyx Silks," October 11-14, Sofiter Raja Orchid, Khon Kaen, Thailand, P63, 2004.
- [4] R. Rajkhowa, Kaur. Jasjeet, Wang. Xungai, and Batchelor, Warren. "Intrinsic tensile properties of cocoon silk fibres can be estimated by removing flaws through repeated tensile tests," *Journal of royal society interface*, 12: 20150177, 2015.H. Poor, *An Introduction to Signal Detection and Estimation*. New York: Springer-Verlag, 1985, ch. 4.
- [5] Treenway Silks. "Silk Yarns, Fibers, Threads & Ribbons". [Online]. [cited 15 November 2018]; Available: <https://www.treenwaysilks.com/productlist.php?secondary=11>
- [6] D., Brahma, Swargiary, A., and Dutta, K. "A comparative study on morphology and rearing performance of *Samia ricini* and *Samia canningi* crossbreed with reference to different food plants," *Journal of Entomology and Zoology Studies* 3(5): 12-19, 2015.
- [7] B., Koç, İ., Eren, and Kaymak, Ertekin, F. "Modelling bulk density, porosity and shrinkage of quince during drying: The effect of drying method," *Journal of Food Engineering*, 85(3), 340-349, 2008.
- [8] Shigley, J.E. and Mischke, C.R. *Mechanical Engineering Design*. 5th Edition. McGraw- Hill Book Company, USA. 1989.

- [9] Krutz, G., Thomson, L., and Claar, P. *Design of Agricultural Machinery*. John Wiley and Sons. New York Chichester Brisbane, Toronto, Singapore, 1994.
- [10] A., N, N, Kakahy, D., Ahmad, M., D, Akhir, S., Sulaiman, and A., Ishak, "Effects of Rotary Mower Blade Cutting Angles on the Pulverization of Sweet Potato Vine," *Agric. Agric. Sci. Procedia*, vol. 2, pp. 95–101, 2014.
- [11] M-S. Huang, K-Y. Chen, and R-F. Fung, "Comparison between mathematical modeling and experimental identification of a spatial slider–crank mechanism," *Applied Mathematical Modelling*, 2010, pp. 2059–2073.
- [12] D.C. Montgomery, *Design and Analysis of Experiment*. 8th ed., John Wiley & Sons, inc., 2013
- [13] D.C. Montgomery, *Design and Analysis of Experiment*. 8th ed., John Wiley & Sons, inc., 2013

A Study on The Effects of Natural-Rubber and Concrete Panel Railroad Crossing Using Finite Element Method

Sirawit Pettrueang and Monsak Pimsarn

*Department of Mechanical Engineering King Mongkut's Institute of Technology
Ladkrabang Bangkok, Thailand*

E-mail: 62601130@kmitl.ac.th and monsak.pi@kmitl.ac.th

Abstract.

Thailand has a railway system with more than 2,500 railroad crossings, and these railroad crossings are generally made of concrete. The truck will reduce speed during passing through to avoid strong vibrations. The material used for comparison with concrete in this research is a rubber compound with a strength additive to absorb the vibration. The chemical composition of the rubber compound is Chloroprene Rubber (CR) 75% and Natural rubber (NR) 25% blended with additives such as carbon black (CB), magnesium oxide (MgO), and sulfur (S8). This research compares the effect on quarter-car models of a truck under dynamic load conditions using the finite element method. The analysis is divided into two steps, as follows: In the first step we applied load, that is unsprung mass and sprung mass of the model, which was obtained from the State Railway of Thailand, and in the second step we set the velocity are 10 km/hr, 20km/hr, 30 km/hr to this quarter-car model. The analyzed results at 10 km/hr, which is the average speed of a vehicle moving through a railroad crossing, showed that the max y-axis displacements of sprung mass when a truck passes through rubber and concrete panels are 11.83 mm, 14.265 mm. the max y-axis displacements of unsprung mass are 14.01 mm, 21.8401 mm. and the internal spring forces are -26,611 N and -29,897 N, respectively but when the truck's velocity increases the rubber panels are more deflated than the concrete panel resulting in the spring force increasing more than the concrete panel.

Keywords. car suspensions systems, quarter-car model, finite element method, hyperelastic material, compound rubber.

1. INTRODUCTION

Thailand is the world's number one primary processing rubber producer and exporter because Thai rubber has high quality and is recognized worldwide. Currently, Thailand has weaknesses or problems with the rubber industry, such as Thailand still relies mainly on rubber exports. when the global economy slows down, it will affect exports to the main markets. The volatility of raw rubber prices is beyond control. and many countries,

especially Cambodia-Laos-Myanmar- Vietnam (CLMV) countries, have started planting more rubber cause the world rubber supply exceeds the demand. Therefore, Thailand must support and promote to use of rubber in the country. Including value-added rubber processing, which will help increase income for farmers.

The railway industry is growing due to investment in rail development in Thailand. That is developing a long-distance railway network from single-way to double-track, covering 47 provinces. So that in the future, the double-track railway will increase to 3,157 kilometers. Currently, there are more than 2,500 railway crossings across the country made of concrete. Therefore, cracking is a disadvantage because concrete is not resistant to repetitive loads, and concrete is a hard and brittle material. When the vehicle passed through the railroad crossing, there was a vibration causing a reduction in driving comfort and loud noise so that the car would reduce speed. All these reasons lead to accidents and cost the repair budget.

For this reason, this research used rubber compounds as an excellent alternative to shocking, and withstand repetitive loads. so the rubber can absorb shock. we study on effects of the Quarter-car model of a truck, which divide the analysis into two steps, that are assigning loads and setting velocity to pass through a railroad crossing for analyzing the y-axis displacement of unsprung mass, the y-axis displacement of the sprung mass, and the internal spring force for comparison between the rubber panel and the concrete panel. If the research is successful, the rubber panel can use instead of the concrete panel. That will result in the value of the domestic rubber industry has increased, designed and produced by Thai companies for value-added rubber processing, which will increase revenue for rubber farmers. and there are also promoting the use of rubber in Thailand.

2. METHODOLOGY

2.1. *Quarter-Car Model*

In order to study the effect of variables in the suspension system of trucks, a quarter-car model is a model that considers only one of the four corners of the car. It is the most widely used model because it has two degrees of freedom, which is easy to calculate because this model consists of only two equations of motion. which is shown in Fig. 1. A quarter-car model is used for this research. The model is determined that the unsprung mass has a mass equal to m_1 , which consists of the mass of the wheel and axle. which is in contact with the rubber pad which has the function of the rubber pad as if there was a spring with the spring stiffness coefficient equal to k_r . The rubber panel has a spring stiffness coefficient that varies with each position. Then, the sprung mass is equal to m_2 , which consists of the mass of the vehicle body and the weight of the driver. which compares the operation of the truck's suspension system as if be spring and a shock absorber with a spring stiffness coefficient and the damping coefficient of the damper were k_2 and c_2 , respectively. Let m_1 , m_2 be a rigid body to make it easier to calculate. And we don't consider the deformation of vehicle body, wheel, axle and tire Therefore, if the tire is a rigid body, we do not need to consider the spring stiffness coefficient and the damping coefficient of the tire in this research.

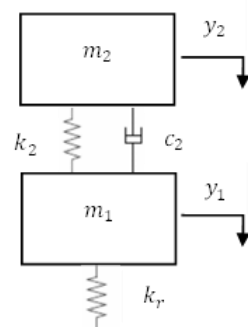


Figure 1 The quarter-car model of the vehicle.

The parameters of the quarter-car model for this research are shown in table 1.

Table 1 The vehicle system parameters for the quarter-car model

Sprung mass	m_2	2250 kg
Unsprung mass	m_1	320 kg
Spring stiffness	k_2	160 kN/m
Damping coefficient	c_2	1500 Ns/m
Rubber pad stiffness	k_r	Variable according to each position of the rubber panel

The mathematical model for the motion of the sprung mass (m_2) and the unsprung mass (m_1) as shown in Fig. 2. and Fig. 3, respectively.

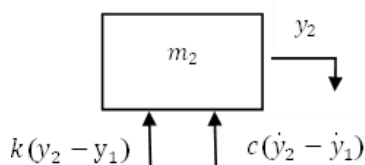


Figure 2 Free Body Diagram of mass m_2 .

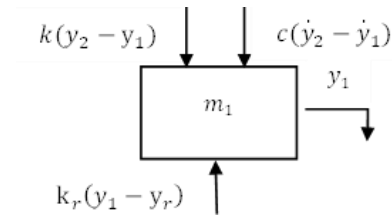


Figure 3 Free Body Diagram of mass m_1 .

The purpose of the modeling was to study the y -axis displacement of the sprung mass and the unsprung mass, and the forces acting on the springs to study the effects of the truck suspension when the truck passed through rubber and concrete panel.

2.2. Material Properties

Initially, we must determine material properties. The compound rubber has been researched and developed a formula to absorb the impact, this rubber panel composition is given in Table 2.

Table 2 Chemical composition of rubber

Ingredient	CR/NR ratio	carbon black	magnesium oxide	sulfur
Composition	75/25	60 phr	1 phr	1 phr

The properties of hyperelastic rubber use Yeoh's model to be considered in this research. The mechanical properties are obtained from the curve fitting value of the tensile test data. As shown in Fig. 4.

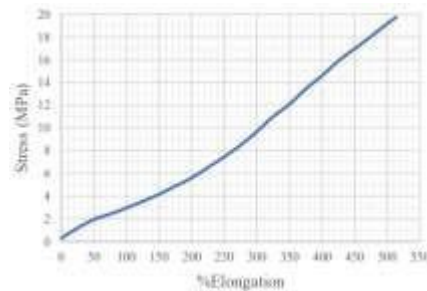


Fig. 4. Tensile test result of rubber.

From the curve fitting process using ANSYS, the Yeoh 3rd order model parameters are $C_{10} = 82.595 \times 10^5$ Pa, $C_{20} = 15.303 \times 10^4$ Pa and $C_{30} = -54.453$ Pa, this constitutive model is given in equation (1).

$$W = C_{10}(I_1 - 3) + C_{20}(I_1 - 3)^2 + C_{30}(I_1 - 3)^3 \quad (1)$$

The components of the model used are shown in fig 4. and mechanical properties of other materials are shown in Table 3.

Table 3 Chemical composition of rubber

material	Ultimate Tensile Strength (MPa)	Yield Strength (MPa)	Young's modulus (MPa)	Poisson's ratio
Structural steel	460	250	20,000	0.3
Concrete	5	0	40,000	0.18

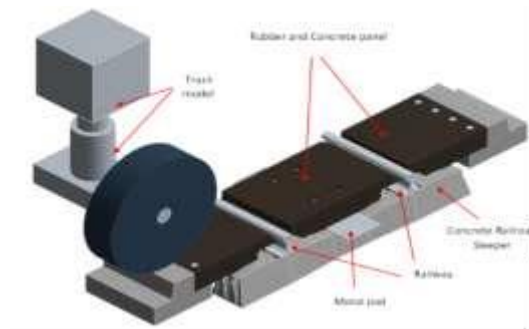


Figure 4 Model components.

2.3. Loading and Boundary condition

The finite element method analysis of 3D problems by ANSYS workbench program. We have divided the analysis into two steps: first step, Assign the load to the model. The load is coming from two parts that are 1. sprung mass. The load value is 22.5 kN, 2. unsprung mass, The load value is 3.2 kN, and the second step. Assign the car to move on the -z-axis at 10km/hr, 20km/hr, and 30km/hr. as shown in fig 5.

The contact relationship of this model has cases that is 1. bonded contact, 2. Rough contact, 3. Frictional contact and 4. frictionless contact. The truck body and wheel on this model are assumed to be a rigid body. We set fixed support at the concrete sleeper, concrete support, and rail. The contact condition and fixed condition are shown in fig. 6 and 7. These settings were set to the same in both the concrete panel and the rubber panels to compare the effects of the truck suspension.

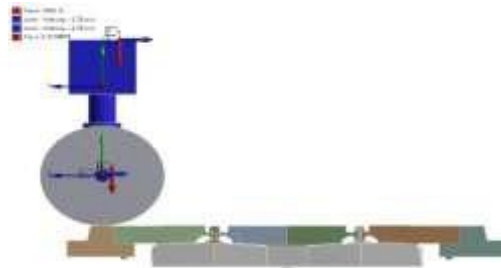


Figure 5 Loading condition

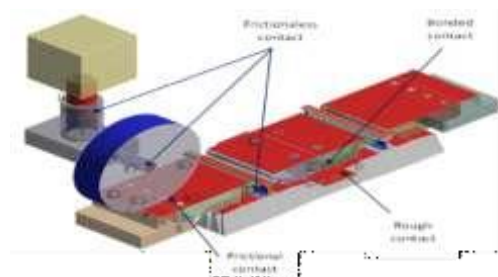


Figure 6 Contact condition.

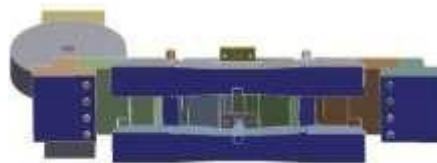


Figure 7 Fixed condition.

3. NUMERICAL SIMULATION

The result is displayed in two steps. The first step is to balance the internal spring force between sprung mass and unsprung mass by setting a step time equal to 2 s, causing the system to enter equilibrium. Then the second step is to determine the duration relative to the speed of the truck, which is 0.98 s, 0.491s, and 0.327s.

The result is as follows: the y-axis displacement of sprung mass, y-axis displacement of unsprung mass, and internal spring force at a speed of 10 km/hr are shown in fig 8,9,10, respectively.

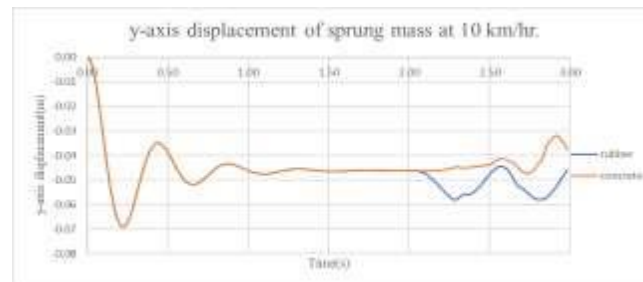


Figure 8 Y-axis displacement of sprung mass at 10 km/hr.



Figure 9 Y-axis displacement of unsprung mass at 10 km/hr

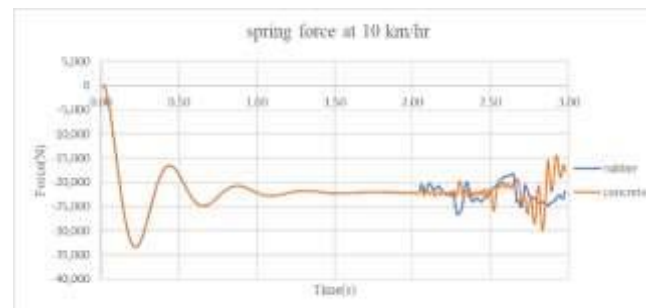


Figure 10 Spring force at 10 km/hr.

Then, we study on the effect of the spring force by analyzing the simulation results in the second step, which this step shows results when the truck passed through the Railroad Crossing in the $-Z$ direction for a distance of 2.725 m. The results were compared between the Rubber Panel and the Concrete Panel at 10km/hr, 20km/hr, and 30km/hr. shown in fig 11,12,13, respectively.

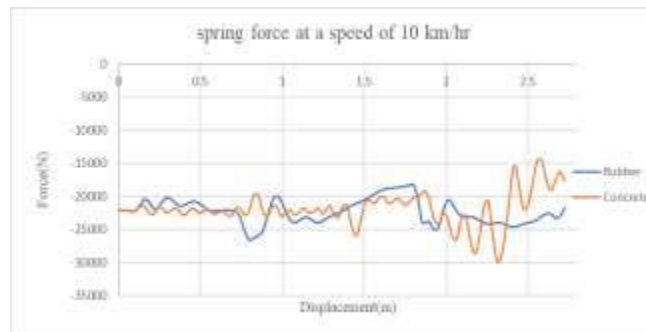


Figure 11 Spring force at 10 km/hr

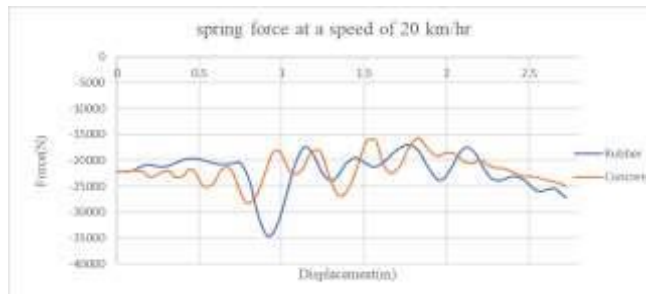


Figure 12 Spring force at 20 km/hr

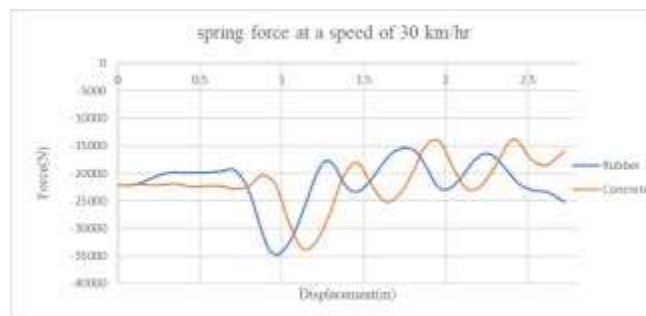


Figure 13 Spring force at 30 km/hr.

From the analysis results, the change in truck speed had a greater effect on the collapse of the rubber panels than the concrete panels. Therefore, the impact of the truck's suspension was analyzed, and compared the y-axis displacement of unsprung mass, and internal spring force when the truck passed through the rubber panel at all three speeds. shown in fig. 14,15, respectively.

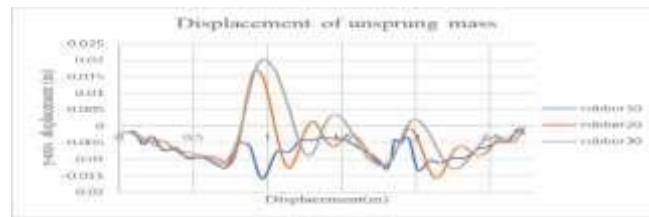


Figure 14 Y-axis displacement of unsprung mass (rubber panel).



Figure 15 Y-axis displacement of sprung mass (rubber panel)

deformation of the external rubber panel shows as a sample because this part is most deflated shown in fig.16. and this reason resulting in the force in the spring is the most valuable when wheel impact with railway shown in fig.17.

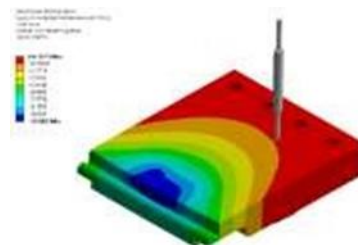


Figure 16 Deformation of external rubber panel

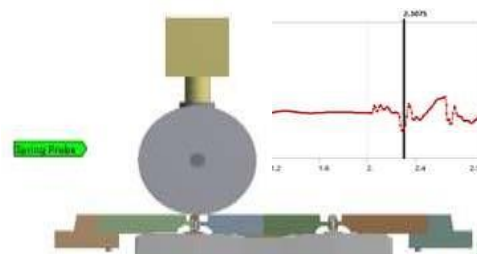


Figure 17 Max spring force at 10 km/hr.

4. CONCLUSIONS

According to the comparison results sample, at 10 km/hr as the average speed of a vehicle passing through Railroad Crossing has approximately 10 km/hr. The data values shown are the values added from the equilibrium point in step 1. as shown in table 4.

Table 4 The simulation result at a speed of 10 km/hr.

Results	Rubber panel	Concrete panel
Max y-axis displacement of sprung mass (mm)	11.83	14.265
Max y-axis displacement of unsprung mass (mm)	14.01	21.8401
Max spring force (N)	-26,611	-29,897

From the analysis results at 10 km/hr, when a truck passed through rubber panels. It appears that the two masses are moving down the collapsing of the rubber panels, which max displacement in the y-axis of the sprung mass and unsprung

mass collapse from the equilibrium point is 11.83 mm, 14.01mm. but when a truck passed through the concrete panel, unsprung masses impact the concrete panel, causing it to bounce back, which max displacement in the y-axis of the sprung mass and the unsprung mass bounce from the equilibrium point is 14.265 mm, 21.84 mm. It was concluded that the maximum displacement of both systems showed that the amplitude of the sprung mass, when passed through the concrete panel, was 20.58% higher than the rubber panel, and the unsprung mass of the concrete panel was 55.89% higher than the rubber panel.

Then considering the spring force when it passed through the rubber panel, the spring force is reduced, but when the truck at the neck of the rubber panel, which has the most collapses. Causing the wheels to impact the railway, and there is bounce. This is the reason why the force in the spring is increased to -26611N, but the concrete panel, when the truck passed through the railway, there is an impact with the concrete panel which is a hard material, resulting in the spring force increases and leads to vibration. The spring force of the system is up to -29897 N, so the spring force of the truck when it passed through the concrete panel was 55.89% higher than the rubber panel.

From the analysis, when considering the impact of the suspension system when the truck passes through the tire panel, it was found that As the truck's velocity increases, the tire panels are more deflated, resulting in the spring forces increase. so that should improve the neck of the rubber panel to collapse less

5. ACKNOWLEDGMENT

We would like to express my special thanks of gratitude to the National Research Council of Thailand and State Railway of Thailand, who always provided information and valuable suggestions

6. REFERENCES

- [1] Z. Yuli, A. Mohammed, B. Fengrong, Parameter identification and robust vibration control of a truck driver's seat system using multi-objective optimization and genetic algorithm, *Applied Acoustics*, Volume 173, 2021, Article 107702
- [2] S. Aunna, I. Sukhom, P. Monsak, C. Jarruwat, T. Veerachai, "Design of natural-rubber panel railroad crossing using finite element method," in ICEAST, 2018.
- [3] M. A. A. Abdelkareem, M. Mostafa, "An analytical study of the performance indices of articulated truck semi-trailer during three different cases to improve the driver comfort," in *Proceedings of the Institution of Mechanical Engineers Part K Journal of Multi-body Dynamics*, 2018.
- [4] Soliman, A., Gazaly, N., and Kadry, F., "Parameters Affecting Truck Ride Comfort," *SAE Technical Paper 2014-01-0147*, 2014
- [5] Abd El-Nasser S. Ahmed, Ahmed S. Ali, Nouby M. Ghazaly, G. T. Abd el- Jaber, "PID CONTROLLER OF ACTIVE SUSPENSION SYSTEM FOR A QUARTER CAR MODEL," *International Journal of Advances in Engineering & Technology*, vol. 8, no. 6, pp. 899-909, 2015.
- [6] S. Kavin, Development of rail pads from chloroprene rubber and natural rubber blend, 110 (2005)
- [7] The state railway of Thailand, NSTDA, KMUTT, NRCT, *The Knowledge Accumulation of Rail Transportation: Case Study of Infrastructure- Basic railway* (2015)
- [8] ISO 2285 international standard "Rubber, vulcanized or thermoplastic - Determination of tension set under constant elongation, and of tension set, elongation and creep under constant tensile load" (2013)
- [9] O. Uwe, P. Martin, S. Eck, W. Daves, *Validation of a finite element crossing model using measurements at an instrumented turnout* (2013)

Thermal Comfort Characteristics Using An Automatic Fan Speed Control And 360° Object Tracking Based On Microcontroller

Jindaporn Jamradloedluk and Songchai Wiriyaumpaiwong

Faculty of engineering Mahasarakham University Maha Sarakham, Thailand

E-mail: jindaporn.j@msu.ac.th and songchai.w@msu.ac.th

Abstract.

Energy saving in residential buildings and global warming situations has a potential to interest of thermal comfort. ASHRAE thermal sensation scale (ASH) is considered the thermal comfort in this work. An automatic speed control and object tracking fan was developed and tested. Field thermal comfort tests both of natural ventilation and air conditioning rooms were also assessed. The results revealed that an automatic fan can function both of speed control and object motion capture with 100% accuracy. This is helpful to enhance thermal comfort for sedentary and non-sedentary activities in daily life. Occupants satisfied in distance not over 1.5 meters and ASH was almost in the neutral zone.

Keywords. object capture, thermal sensation scale, sedentary activity, variable fan speed, Arduino.

1. INTRODUCTION

Thailand is a country in Southeast Asia, located at the northern hemisphere. The average maximum temperature in the hot season can be reach to 35°C. Especially, the northeast region of Thailand climate all year round is almost hot and humid, except between mid-November and mid-February. The people feel bad in this time interval. A solution of more comfortable feeling is always turning on a fan.

The fan evolution is now happened in many versions. It is designed by criteria of air flow rate, air pressure, and user purposes, e.g., centrifugal, axial, pedestal, ceiling, table, tower, misting, and evaporative cooling fans. A kind of fan, pedestal fan, is often seen in household appliances.

Recently tropical climate researches mostly studied the effect of air movement by fan assisted air conditioning on thermal comfort for many activities, e.g., classrooms, laboratories, sedentary and non-sedentary office activity levels, living room and bedroom [1-7].

The experimental airflow is classified as three main patterns: constant mechanical, pulsating, and sinusoidal. Increased airflow in indoor space led to increased mean and standard deviation of air speed but decreased mean and standard deviation of turbulence intensity when compared to without sources of increased airflow or natural ventilation [8]. The sinusoidal pattern at more than 40% turbulence intensity, the 0.5-1.0 Hz fluctuation frequency and a constant 0.6 m/s average air speed under condition of 28-30°C and a constant 35% RH, is studied in 2012 [9]. The thermal sensation vote (TSV) showed that human feel cool at the 28°C air temperature whilst, feel hot at the 30°C air temperature with a range of 0.5-1.0 Hz frequency. Later in 2018, intensified global warming periods, human feel cool at lower than 25°C (air temperature decreased around 3°C from 2012) while feel comfort at 25°C under condition of 50-70% RH, 0.2-0.6 m/s and 0.016-0.1 Hz [10].

Additionally, the constant mechanical and pulsating patterns (turbulence intensity < 40%) and sinusoidal pattern (turbulence intensity > 40%) at a constant condition: 27.5°C, 50% RH, and 0.65 m/s is compared on thermal comfort. TSV vote of the constant mechanical and sinusoidal patterns are positive (slightly hot) and negative (slightly cool) for pulsating pattern [11].

The people would like decrease the air velocity after 30 minutes exposure in variable airflow direction [12]. The comfortable air speeds are between 0.25 m/s (at 27°C and 40%-60% RH) and 1.17 m/s (at 30°C and 60%-80% RH) and between 0.12 m/s and 1.31 m/s for 2 beds of healthy young people in the 20 m² bedroom area with pedestal fan coupled with 3500 W air conditioner [7]. The optimized air movement in University classroom can enhance the thermal comfort satisfaction from 62% to 94% of totally 34 persons [13].

The current deteriorated developing global recession resulted in the reduction of net income. Many undergraduate students necessary to select the lowest cost of accommodation by renting fan room with natural ventilation (no air conditioner). They feel hot in summer season, therefore, this study aims to develop and build a 360° object tracking fan to enhance thermal comfort of student's accommodation. The thermal comfort under pedestal fan speed control complied with air temperature and relative humidity was also studied in student's accommodation and air conditioning faculty office.

2. MATERIALS AND METHODOLOGY

2.1 Design Principles

A pedestal fan is design by using 6 sets of ultrasonic sensor HC-RS04 (working temperature: -15°C to 70°C, sensing angle: 30° cone, angle of effect: 15° cone, and ultrasonic frequency: 40kHz) for detecting the object tracking and a sensor module DHT22 (measured temperature range of -40 to 80°C with ± 0.5°C accuracy) for measuring and displaying the air temperature and humidity. We used the Arduino Uno R3 microcontroller board for controlling the operation of 360° object tracking by stepping motor and variable air velocity with air temperature and relative humidity.

2.2 Accuracy Test

A prototype of 360° object tracking fan as Fig. 1 is tested in 6 different directions of ultrasonic sensor and 3 different levels of distance between sensor and object: 0.5, 1.0, and 1.5 meters.

The variable air speed testing, fan speed level is adjusted corresponding to air temperature and relative humidity condition as shown in Table 1.

2.3 Field thermal comfort

The operation testing of 360° object tracking and variable fan speed starts from 2 students came in their accommodation (2 beds fan room size: 20 m² and opening space for 2 windows with natural ventilation) and fill thermal sensation scale questionnaire. Each student was done for 3 time intervals: morning (9 AM-11 AM), afternoon (12 PM-2 PM), and evening (4 PM-6 PM) in the same day. The temperature and relative humidity of air in tested room and fan speed number is recorded in every 10 minutes for each time interval. At a 64 m² equipped 2 sets of 1 tons air conditioning faculty office, we have test in the morning and afternoon. Thermal comfort is assessed by ASHRAE thermal sensation scale (ASH). This scale is divided into 7 levels of -3 to 3 as presented in Fig. 2.

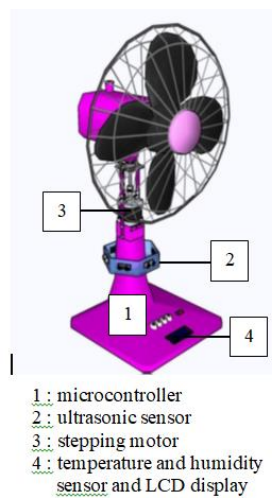


Figure 1 A fan speed control and 360° object tracking based on microcontroller.

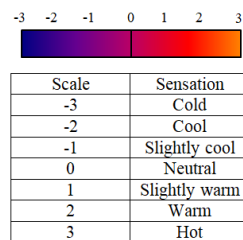


Figure 2 ASHRAE thermal sensation scale.

Table 1 Criteria for adjusting fan speed level

Room condition	fan speed level
T < 25°C, RH<70%	No. 0
T 25-29.9°C and RH<70%	No. 1
T 30-33.9°C and RH< 70%	No. 2
T ≥ 34°C and RH< 70%	No. 3
T 25-27.9°C and RH≥70%	No. 2
T 28-32°C and RH≥70%	No. 3

3. RESULTS AND DISCUSSION

3.1 Accuracy test of the direction sensor

Ultrasonic sensor was turned towards 6 different directions to detect moving and static objects at the radii of 0.5, 1.0 and 1.5 m. The accuracy tests of the direction sensor showed that 100% accuracy was achieved at the distance of 0.5 and 1.0 m. However, the accuracy slightly dropped at 1.5 m.

3.2 Accuracy test of the temperature and relative humidity sensor

DHT22 Temperature & Relative Humidity Sensor was used as a key component of the developed automatic fan. It could automatically change the fan speed according to the set temperature and relative humidity. The accuracy tests of the sensors were conducted in triplicate. The test results were tabulated in Table 2. It is clearly seen that the sensors could completely control the fan speed level in accordance with the specific conditions.

3.3 Thermal comfort via thermal sensation scale (ASH)

The ASHRAE thermal sensation scale was developed for use in quantifying people's thermal sensation. The sensation scale expressed from -3 to +3 corresponding to the categories "cold (-3)," "cool (-2)," "slightly cool (-1)," "neutral (0)," "slightly warm (1)," "warm (2)," and "hot (3)." [14]. People voting +2, +3, -2, or -3 on the thermal sensation scale are assumed that they feel uncomfortable.

The experiments were performed in the summer of Thailand (March – April 2020) at three time intervals viz. in the morning (9 AM – 11 AM), in the afternoon (12 PM – 2 PM), and in the evening (4 PM – 6 PM). During the day, air temperature tended to increase whilst the relative humidity tended to decrease. At 9 AM to 11 AM, air temperature gradually increased from 29°C to 33°C and relative humidity drastically decreased from 72% to 62%. Mean value of ASH (ASHRAE thermal sensation scale) in Fig. 3 illustrated that at the beginning of the experiment, the occupants felt slightly warm and then they felt indifferent. Generally, tropical climatic regions have high temperature and humidity levels in the summer season. However, in the morning interval of this research work, the level ranges are not an extreme condition therefore the feeling is mostly in neutral sensation. Most of temperature and relative humidity are in the air conditioned zone [15].

Additionally, it was depicted in Fig. 4 that at 12.00 PM to 12.20 PM the thermal sensation scale was 1 (Slight warm). After that, the fan speed level was automatically elevated from 2 to 3. This led to the neutral preference during 12.30 PM – 12.50 PM. Nevertheless, after 01.00 PM the temperature gradually increased and reached 35°C at 01.20 PM. Such a relatively high temperature resulted in the positive side of thermal sensation scale.

As depicted in Fig. 5, during 4 PM – 4.30 PM, thermal sensation was considered slightly warm (1) and warm (2). Thereafter, the air temperature seemed to be maintained at 34°C. Although the air temperature is rather high, thermal sensation was still in the neutral zone. This was because the fan speed level was automatically changed from speed level 2 to speed level 3. The increased air velocity resulted in the pleasant feeling. Furthermore, occupants felt more comfort for an automatic fan than the general electric fan, especially in case of non-sedentary activities in fan room.

The experiments of variable fan speed in air conditioning faculty office were executed in the summer of Thailand (mid-April 2020) in the morning (9 AM – 11 AM) and in the afternoon (12 PM – 2 PM) as shown in Fig. 6-7. The ambient air temperature tended to increase whilst the relative humidity tended to decrease during the day. At 9 AM to 11 AM, room temperature gradually decreased from 30°C to 25°C (set point temperature of air conditioner) and room relative humidity drastically decreased from 70% to 46%. Mean value of ASH at the beginning, the occupants felt slightly warm and then they felt comfort - slightly cool - cool at 30, 50, and 60 minutes, respectively

In the afternoon 12.00 PM to 12.20 PM, the thermal sensation scale was 1 (Slight warm) and then the fan speed level was automatically stepdown from 2 to 1. This led to the neutral preference during 12.30 PM – 02.00 PM. Nevertheless, the room temperature gradually decreased and reached 25°C at 01.00 PM. Such a relatively mild temperature resulted in the comfortable thermal sensation scale.

Table 2 Accuracy of the fan speed level according to the specific conditions

The given conditions	Fan speed level	Accuracy
$T < 25^{\circ}\text{C}$, $\text{RH} < 70\%$	No. 0	100%
$T = 25\text{-}29.9^{\circ}\text{C}$, $\text{RH} < 70\%$	No. 1	100%
$T = 30\text{-}33.9^{\circ}\text{C}$, $\text{RH} < 70\%$	No. 2	100%
$T > 34^{\circ}\text{C}$, $\text{RH} < 70\%$	No. 3	100%
$T = 25\text{-}27.9^{\circ}\text{C}$, $\text{RH} \geq 70\%$	No. 2	100%
$T = 28\text{-}32^{\circ}\text{C}$, $\text{RH} \geq 70\%$	No. 3	100%

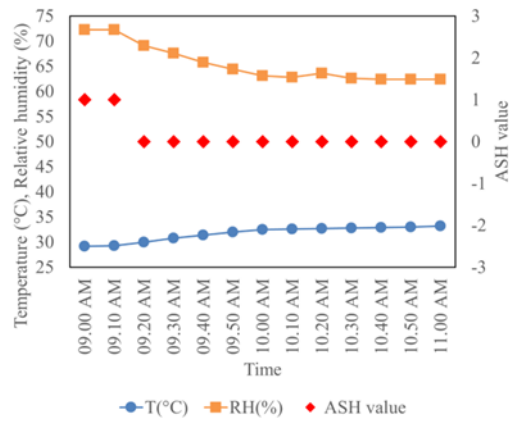


Figure 3 Temperature and relative humidity of the air and thermal sensation scale voted by occupants in the morning period of fan room student’s accommodation

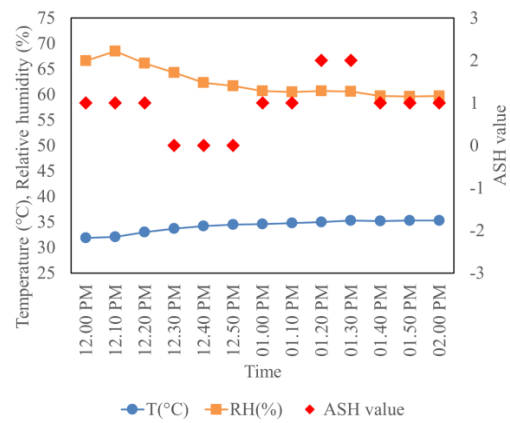


Figure 4 Temperature and relative humidity of the air and thermal sensation scale voted by occupants in the afternoon period of fan room student’s accommodation.

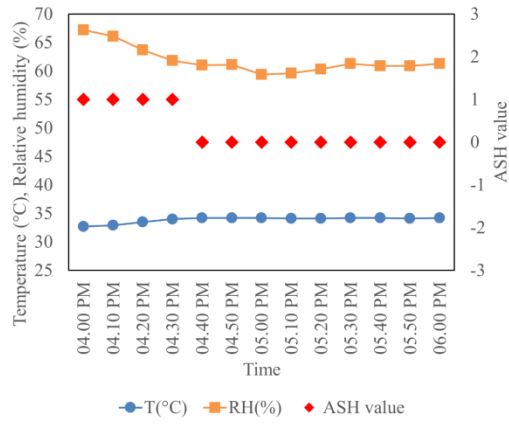


Figure 5 Temperature and relative humidity of the air and thermal sensation scale voted by occupants in the evening period of fan room student’s accommodation.

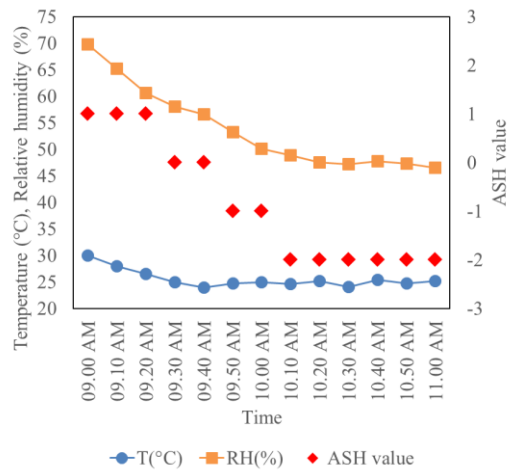


Figure 6 Temperature and relative humidity of the air and thermal sensation scale voted by occupants in the morning period of air conditioning faculty office.

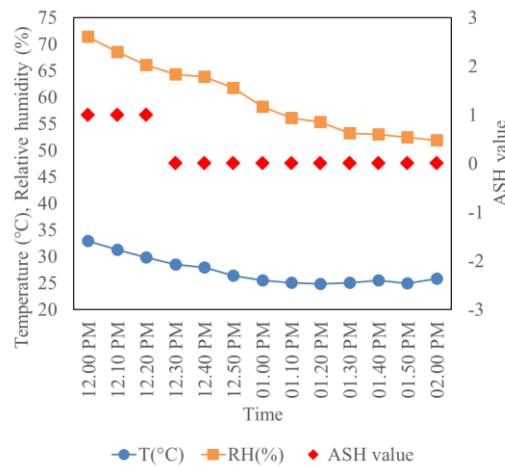


Figure 7 Temperature and relative humidity of the air and thermal sensation scale voted by occupants in the afternoon period of air conditioning faculty office

4. CONCLUSIONS

An automatic fan was developed and tested in this research work. The fan could automatically turn to the direction of object existence with almost 100% accuracy. In addition, it could automatically adjust the speed level according to the temperature and humidity of the surrounding air. Thermal comfort via thermal sensation scale indicated that when temperature and relative humidity were in the uncomfortable condition, the fan would automatically speed up. Consequently, thermal sensation scale were mostly in the neutral zone. The tests in other case, air conditioning faculty office, this developed fan could help to enhance the airflow movement and comfortable preference.

5. ACKNOWLEDGMENT

We would thank faculty of engineering, Maharakham University for financial and facilitated supports.

6. REFERENCES

- [1] N. Puangmalee, K. Hussaro, V. Boonyayothin, and J. Khedari, "A Field of the Thermal Comfort in University Buildings in Thailand under Air Condition Room," *Energy Procedia*, vol. 79, 2015, pp. 480-485.
- [2] A. Lipczynska, S. Schiavon, and L.T. Graham, "Thermal comfort and self-reported productivity in an office with ceiling fans in the tropics," *Build Environ.*, vol. 135, 2018, pp. 202-212.

- [3] Y. Zhai, E. Arens, K. Elsworth, and H. Zhang, "Selecting air speeds for cooling at sedentary and non-sedentary office activity levels," *Build Environ.*, vol. 122, 2017, pp. 247-257.
- [4] S. Tadepalli, T.K. Jayasree, V.V. Lakshmi, and S. Chelliah, "Influence of ceiling fan induced non-uniform thermal environment on thermal comfort and spatial adaptation in living room seat layout," *Build Environ.*, vol. 205, 2021, 108232.
- [5] R. Risetto, M. Schweiker, and A. Wagner, "Personalized ceiling fans: Effects of air motion, air direction and personal control on thermal comfort," *Energy Build.*, vol. 235, 2021, 110721.
- [6] A.K. Mishra and M. Ramgopal, "Thermal comfort field study in undergraduate laboratories - an analysis of occupant perceptions," *Build Environ.*, vol. 76, 2014, pp. 62-72.
- [7] Y. Chen, Y. Zhang, and H. Tang, "Comfortable air speeds for young people lying at rest in the hot-humid area of China in summer," *Build Environ.*, vol. 124, 2017, pp. 402-411.
- [8] Y. Zhang, Q. Liu, and Q. Meng, "Airflow utilization in buildings in hot and humid areas of China," *Build Environ.*, vol. 87, 2015, pp. 207-21.
- [9] L. Huang, Q. Ouyang, and Y. Zhu, "Perceptible airflow fluctuation frequency and human thermal response," *Build Environ.*, vol. 54, 2012, pp.14-19.
- [10] Y. Xie, S. Fu, C. Wu, and C.Y.H.H. Chao, "Influence of sinusoidal airflow and airflow distance on human thermal response to a personalized ventilation system," *Indoor Built Environ.*, vol. 27, 2018, pp. 317-330.
- [11] T. Parkinson and R. de Dear, "Thermal pleasure in built environments: spatial alliesthesia from air movement," *Build Res. Inf.*, vol. 45, 2017, pp.320-335.
- [12] F. Kalm'ar, "Impact of elevated air velocity on subjective thermal comfort sensation under asymmetric radiation and variable airflow direction," *J. Build Phys.*, vol. 42, 2018, pp. 173-193.
- [13] S. Liu, L. Yin, S. Schiavon, W. Khuen, and K.V. Ling, "Coordinate control of air movement for optimal thermal comfort," *Sci. Technol. Built Environ.*, vol. 24, 2018, pp. 886-896.
- [14] ANSI/ASHRAE Standard 55-2017, *Thermal Environmental Conditions for Human Occupancy*.
- [15] G. Baruch, "Comfort, Climate Analysis and Building Design Guidelines." *Energy Build.*, vol. 18(1), 1992, pp. 11-23.

Automatic Shrimp Size Measurement for Pacific White Shrimp Farming Industry Using Artificial Intelligence

Charoen Vongchumyen, Nachaphat Ainthong, Poramee Chansuksett,
Charita Suranantajak

*Department of Computer Engineering, School of Engineering King Mongkut's Institute of
Technology Ladkrabang Bangkok, Thailand*

*E-mail address: charoen.vo@kmitl.ac.th, 61010279@kmitl.ac.th, 61010627@kmitl.ac.th,
61010216@kmitl.ac.th*

Abstract.

The objective of this project is to build an automatic shrimp size measurement machine. The method that farmers currently use to measure the size is to use a fishing net to catch shrimps. This method will cause injuries and accidents to the shrimp. To solve this problem, we design an automatic shrimp size measurement machine to help measure the shrimp safely. The machine will have a plate to catch and raise shrimp above the water surface. The machine's camera will then capture a shrimp image on the plate and send it to a deep learning algorithm to analyze and evaluate shrimp size.

Keywords. Pacific White Shrimp, Deep Learning, Object Detection.

1. INTRODUCTION

At present, the Thai vannamei shrimp farming industry generates a lot of income for the country. In 2019, Thailand produced more than 260,610.08 tons of white vannamei shrimp in the farm system, and exported more than 134,737.85 tons, worth 39,815.52 million baht [1]. In terms of production and exports, lifting the shrimp up to measure the size is one of the reasons for a large reduction in output because shrimp is fragile and must be in the water at all times. Lifting it up will expose the shrimp to air exposure and other stimuli, but the raising of white vannamei shrimp is necessary to provide the right amount of food for each stage of the shrimp age. In addition, human labor is scarce, expensive, and labor's skills cannot be controlled either by looking at the size with the naked eye and on cleanliness.

Therefore, if there is research and development of automatic white shrimp size measurement, Vannamei can make Farmers can greatly reduce their labor usage. In addition, production costs can be directly reduced, and the exact size of white vannamei shrimp can

be realized without direct contact with the shrimp. Make feeding possible most appropriate for each age group resulting in higher efficiency and productivity in production.

2. THEORY AND RELATED RESEARCH

2.1. *Characteristics and rearing of white vannamei shrimp*

Vannamei white shrimp [2] is a Pacific marine shrimp species. Scientifically known as *Litopenaeus vannamei* or *Penaeus vannamei*, it is widely cultivated in many countries due to its vigorous nature. In Thailand nowadays, Thai farmers tend to raise this type of shrimp. Because it is a fast growing shrimp species and takes a short time to raise. General characteristics of white vannamei shrimp The body is white with 8 segments and one segment of the head. The greek is triangular. reddish brown Shrimp intestines can be clearly seen. And when adults are 9 inches long, they are fast moving shrimps. Able to adapt to salinity in a wide range from 3-35 parts per thousand, can eat many types of food. Therefore, it grows and adapts to dense development culture in deteriorated pond conditions better than black tiger shrimp. White Vannamei Shrimp can be raised in both natural systems and semi-dense system This type of shrimp can be familiar with and adjust the habits under various aquaculture systems well. It has a habit of being sensitive to changes in water conditions in the pond. and easily startled Farmers need to have a good farm management system in order to produce good yields in large quantities. The proper form of shrimp farming depends on the location of the farm and on management issues and disease outbreaks that may arise during raising. The development of white shrimp farming in Thailand prefers to use coastal areas or areas with access to sea water. The pond used for raising at present is a rectangular pond. The width and length are not much different. Currently, there are 2 types of popular styles, which are clay ponds and polyethylene fabric ponds.

2.2. *The size according to the age of the shrimp is important to the amount of feeding*

Food is an important factor in successful shrimp farming. Therefore, it is necessary to manage the nutrients and the amount of food that the shrimp will receive appropriately (Table I). divided by the weight or size of the shrimp itself Developed shrimp farming It is commonly used as a readymade pellet food. The deterioration of the shrimp pond was caused by poor feeding management leading to accumulation of food waste from the chin and excreta. There were continual problems concerning raising management and preparation of the pond to have a suitable environment. In addition, shrimp production costs come from feed, approximately 50-60%. Mismanagement of feed that leads to too high a meat exchange rate increases feed costs. Therefore, good shrimp feeding management is necessary to The most efficient shrimp production. The criteria used must ensure that the shrimp are fed the right amount of food at the right time. Every meal during the party The rate of feeding depends on the amount of food you eat. growth rate and shrimp mortality feeding too little causing the shrimp to grow slowly and causing cannibalism especially high-density shrimp farming overfeeding causing the quality of water and soil to deteriorate This made the stressed shrimp weak and the chance of infection with shrimp disease increased. and the growing bacteria use insufficient oxygen in the water for shrimp growth. Daily amount of food Calculated from shrimp quantity and feed rate [2] are: Feed amount (kg/day) = total

shrimp quantity \times percentage feeding / 100, Total shrimp volume (kg) = total shrimp in pond \times average weight, Total number of shrimp in the tank = number of shrimp released \times percent survival / 100

Table 1 Feeding rates according to shrimp weight

Average weight of shrimp (g.)	Feeding rate (% of weight / day)	Average weight of shrimp (g.)	Feeding rate (% of weight / day)	Average weight of shrimp (g.)	Feeding rate (% of weight / day)
< 1	35-25	5.0-5.9	5.5-5.0	13.0-13.9	3.0-2.75
0.1-0.24	25-20	6.0-6.9	5.0-4.5	14.0-14.9	2.75-2.5
0.25-0.49	20-15	7.0-7.9	4.5-4.25	15.0-15.9	2.5-2.3
0.5-0.9	15-11	8.0-8.9	4.25-4.0	16.0-16.9	2.3-2.1
1.0-1.9	11-8	9.0-9.9	4.0-3.75	17.0-17.9	2.1-2.0
2.0-2.9	8-7	10.0-10.9	3.75-3.5	18.0-18.9	2.0-1.9
3.0-3.9	7-6	11.0-11.9	3.5-3.25	19.0-19.9	1.9-1.8
4.0-4.9	6-5.5	12.0-12.9	3.25-3.0	20.0-20.9	1.8-1.7

2.3. RetinaNet

RetinaNet [3] is a simple one-stage model unlike Faster R- CNN or Yolo, it uses Feature Pyramid Network (FPN) [4] (Fig. 1). It detects objects based on multiple scaled image data to improve detection accuracy but takes more time and memory than other detection models to create images of different sizes. RetinaNet performs two functions: 1) identifying what is inside the frame of detection and 2) analyzing the built frame of detection against the ground truth.

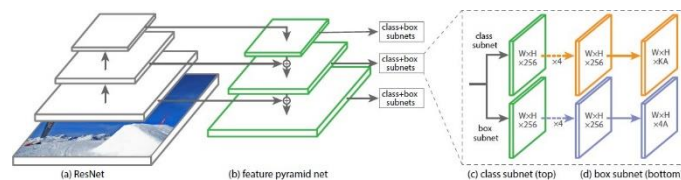


Figure 1 Architecture of RetinaNet [3]

2.4. *Shrimp size measurement method*

To measure the shrimp size, we have to detect the shrimp inside the picture that we captured. We use RetinaNet to detect the shrimp. After that, we can use similar triangle properties to calculate the shrimp size.

3. THEORY AND RELATED RESEARCH

3.1. *Main structure of the machine*

We use PVC pipe as the main structure of the machine which is lightweight, durable and does not erode in saltwater conditions. In addition, the PVC pipe is cheap and easy to buy compared to stainless steel and aluminum (Fig. 2).

For buoyancy, we use floating foam attached to the frame on all sides to help keep the machine balanced. And we use a square shape to maintain balance when the waves hit the machine

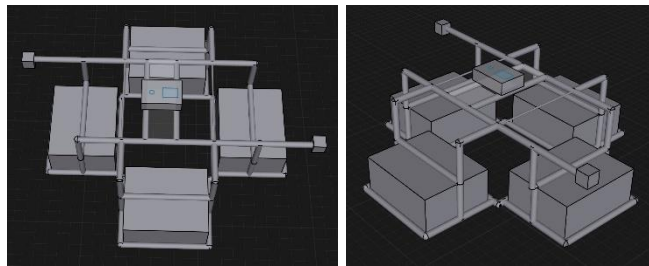


Figure 2 3D model of the machine.

3.2. *The shrimp net and motor system*

We use an acrylic sheet (Fig. 3) for the shrimp net because it has a smooth surface, making the shrimp size calculation process easier. But the acrylic sheet will not drain water, so we drill holes on the sheet, allowing the water to drain and reducing the water pressure when lifting. For the motor system, we use 2 motors to control the shrimp net on the left and right sides. When the system sends a command to lift

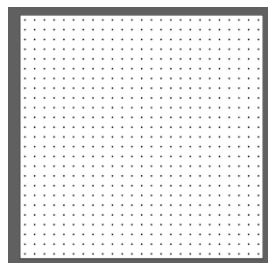


Figure 3 Acrylic sheet design for the shrimp net

the net, both motors will be activated. And when we want to release the shrimp, the motor will tilt the net to one side for the shrimp to be released.

3.3. *Processing system and control unit*

The automatic shrimp scale processing system is based on the Raspberry Pi. Raspberry Pi is the most popular single-board computer that is widely available and small. It can also be connected to the camera of the Raspberry Pi, allowing to take pictures of the shrimp and the shrimp size can be measured locally after imaging. The camera system and the Raspberry Pi are packaged in a water and dust resistant case, which can prevent salt vapor from the shrimp pond. The bottom box is transparent so that the camera can take pictures. Which will use a glass coating that is resistant to salt vapor.

3.4. *The detecting and measuring shrimp size*

In this paper, we have developed a system to detect and measure the size of shrimp. The image obtained from the shrimp imaging was used to detect the shrimp inside the image using RetinaNet, an object detection model. The captured shrimp was analyzed to measure the size of the shrimp by image processing technique.

Developing a RetinaNet model requires the preparation of images before using images to teach the model using the fastNIMeansDenoisingColored [5] technique. It is a technique for reducing noise by adjusting the colors around each point of the colored pixel, which is better than image segmentation with KMean clustering. The image is scaled to fit the model, with the result of the RetinaNet model being the coordinates of the shrimp in Fig. 4

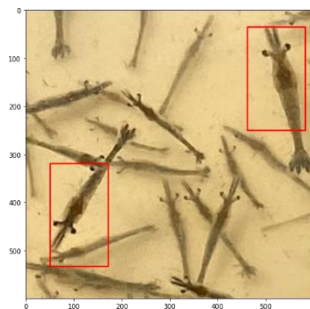


Figure 4 Detect shrimp in images with RetinaNet

Shrimp size measurement uses image processing to analyze the image data to obtain the length of shrimp within the image captured by using RetinaNet. The initial analysis step is the preprocess data.

Preparing the image before being analyzed to measure the size of the shrimp inside the image will convert the RGB image to a grayscale image. It is easy and convenient to analyze by reducing the data size from RGB 3 channel color image to 1 channel grayscale image, reducing processing time and power of computing. The grayscale image is then blurred to

reduce the details of the image to make it easier to see the shrimp inside the image and to reduce noise, making it easier for further analysis (Fig. 5).

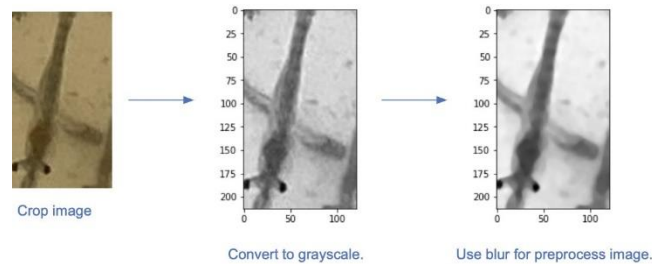


Figure 5 Convert RGB image to Grayscale image and use blur with shrimp image

Once the image preparation is complete, we will separate the shrimp image from the background of the image. It uses an Adaptive threshold [6] algorithm for filtering image data between objects and backgrounds. This allows us to get a black and white image that clearly distinguishes the subject and the background of the image. After obtaining an image that distinguishes the object and its background, two methods were used to measure the size of the shrimp.

- 1) Shrimp size was measured by using a shrimp image that was separated from the object and the background and then finding the points on the shape of the shrimp using the findContours [7] algorithm.
- 2) Shrimp size was measured by using a shrimp image isolated from object and background and then used to find the bones of the image by thinning technique [8], [9]. It finds the object's axes within the image before using the findContour algorithm to find points on the shape of the shrimp.

We will use those points to find the points that are farthest apart when forming a straight line to get the shrimp's longest straight line. The shrimp's longest straight line assumes that line is the one that passes through the shrimp's rostrum and telson, which is the size of that shrimp (Fig. 6).

4. EXPERIMENTAL RESULT

Development of an automatic shrimp size measurement as mentioned in the Methodology section. It consists of photo-graphic equipment and a system for measuring the size of shrimp. The results are as follows.

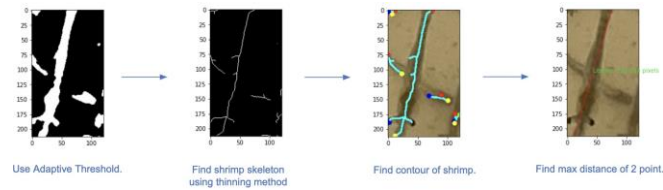


Figure 6 Flow of find shrimp's length

4.1. *Automatic shrimp size measurement machine*

We've built the machine as designed on the 3D model but we've reduced the size of the machine to better suit real-world usage (Fig. 7).



Figure 7 The shrimp size measurement machine

4.2. *Result from the detecting and measuring shrimp size*

Performance testing of the shrimp detection system within the image with RetinaNet. It was found that the RetinaNet model was able to detect shrimp inside the image (Fig. 8a), but was less effective when the image was noisy and underexposed (Fig. 8b). We trained the model with 300 shrimp pictures and validate it with 100 shrimp pictures, then we took the trained model to test with a test set that contains 100 pictures. The precision, recall, and F1 score value from IoU of the model is 57.28%, 31.98%, and 41.04% respectively, which we're focusing on the precision value because detecting only some of the shrimp is sufficient enough to measure the overall shrimp size.

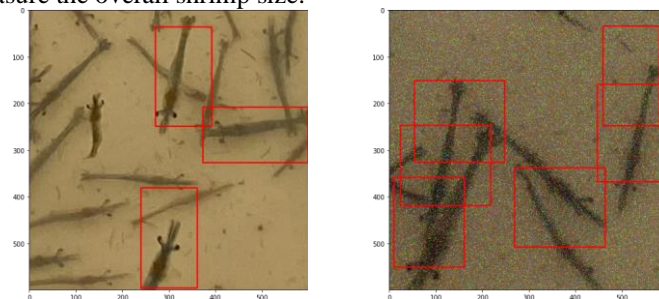
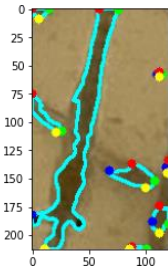
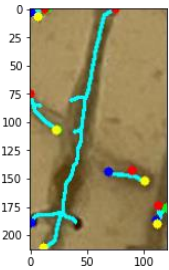
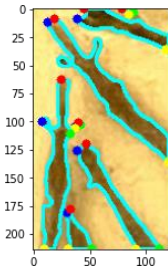
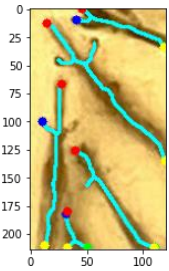


Figure 8 Shrimp Detection Test Pictures

From testing the efficiency of shrimp size measurements using various techniques, the results were as follows in Table II

Table 2 Table comparing the efficiency of shrimp length determination using different techniques

Contour technique	Contour technique with Thinning
	
	

According to the results, the contour technique together with thinning [8], the shape of the shrimp can be seen effectively. Using thinning will help to find the shape of the shrimp better.

5. CONCLUSION

The automatic shrimp size measurement machine is capable of measuring shrimp size efficiently by taking shrimp pictures. The machine relies on object detection technology to detect shrimp, and the machine uses the information to analyze shrimp size. The machine collects pictures at a specified time every day, then calculates an average shrimp size using the pictures. This will let users know the proper amount of shrimp food, and as this process is fully automatic, it can reduce human workers. This automatic shrimp size measurement machine consists of two components: The shrimp net controller component: It uses two motors to lift the shrimp and release it by tilting the net to one side. The detecting and measuring shrimp size component: The process starts from taking a shrimp picture and pre-processing it. After that, the picture will get into the object detection process using RetinaNet. When completed, we will crop it to measure shrimp size by using thinning to find the skeleton and then take the information to compute contour to calculate the shrimp size. The precision value from the RetinaNet model, which was trained by 300 shrimp

pictures and tested with 100 pictures, is 57.28%. We believe that the performance can be improved further by increasing training set pictures and tuning parameters.

6. REFERENCES

- [1] Fisheries Economics Division, Department of Fisheries, “Sea shrimp situation report in 2019 and trends in 2020.” [Online]. Available: <https://www.fisheries.go.th/strategy/fisheconomic/Monthly%20report/Shrimp/1%E0%B8%81%E0%B8%B8%E0%B9%89%E0%B8%87%E0%B8%97%E0%B8%B0%E0%B9%80%E0%B8%A5%20%2012%20%E0%B9%80%E0%B8%94%E0%B8%B7%E0%B8%AD%E0%B8%99%2062.pdf>
- [2] R. Fauzi, A. Pamungkas, and D. Purwadi, “White Shrimp *Litopenaeus vannamei* Based Agroindustry Through Recirculating Aquaculture System to Increase Competitiveness,” *E3S Web of Conferences*, vol. 147, p. 01002, Jan. 2020.
- [3] T.-Y. Lin, P. Goyal, R. Girshick, K. He, and P. Dollár, “Focal Loss for Dense Object Detection,” *arXiv:1708.02002 [cs]*, Feb. 2018, *arXiv: 1708.02002*. [Online]. Available: <http://arxiv.org/abs/1708.02002>
- [4] T.-Y. Lin, P. Dollár, R. Girshick, K. He, B. Hariharan, and S. Belongie, “Feature Pyramid Networks for Object Detection,” *arXiv:1612.03144 [cs]*, Apr. 2017, *arXiv: 1612.03144*. [Online]. Available: <http://arxiv.org/abs/1612.03144>
- [5] “OpenCV: Denoising.” [Online]. Available: https://docs.opencv.org/3.4/d1/d79/group_photo_denoise.html
- [6] “OpenCV: Miscellaneous Image Transformations.” [Online]. Available: https://docs.opencv.org/4.x/d7/d1b/group_imgproc_misc.html
- [7] “OpenCV: Structural Analysis and Shape Descriptors.” [Online]. Available: https://docs.opencv.org/3.4/d3/dc0/group_imgproc_shape.html
- [8] Y. He, S. H. Kang, and L. Alvarez, “Finding the Skeleton of 2D Shape and Contours: Implementation of Hamilton-Jacobi Skeleton,” *Image Processing On Line*, vol. 11, pp. 18–36, 2021.
- [9] “Skeletonize — skimage v0.19.2 docs.” [Online]. Available: https://scikit-image.org/docs/stable/auto_examples/edges/plot_skeleton.html

Author index

A

Ainthong, Nachaphat 59

C

Chansuksett, Poramee 59

Chueycham, Supatta 11

Chupayak, Jakkapong 11

J

Jamradloedluk, Jindaporn 50

K

Kansuwan, Panya 1

Kreetachart, Torpong 11

M

Manonukul, Anchalee 1

P

Pahasup-anan, Taddao 11

Petrueang, Sirawit 39

Pimsarn, Monsak 39

Poolchantakorn, Phisuttinee 11

Poomsa-ad, Nattapol 22

Promthaisong, Pitak 31

S

Sucharitpwatskul, Sedthawat 1

Supina, Preecha 11

Suranantajak, Charita 59

Suwannahong, Kowit	11
T	
Tesiri, Oumaporn	11
Toong-ood, Kaned	31
V	
Vongchumyen, Charoen	59
W	
Weerayuth, Nantawatana	31
Wiriyaumpaiwong, Songchai	50
Wiset, Lamul	22
Wongcharee, Surachai	11
Wongcharee, Surachai	31
Wongkasem, Kasorn	31
Y	
Youichi Kempimook, Brian	11

i⁸th C^{east} 2022

Chiang Mai, Thailand

